22. Hedelin M, Klint A, Chang ET, Bellocco R, Johansson JE, Andersson SO, Heinonen SM, Adlercreutz H, Adami HO, et al. Dietary phytoestrogen, serum enterolactone and risk of prostate cancer: the cancer prostate Sweden study (Sweden). Cancer Causes Control. 2006;17:169–80.
23. Sonoda T, Nagata Y, Mori M, Miyanaga N, Goto K, Naito S, Fujimoto K, Hirao Y, Takahashi A, et al. A case-control study of diet and prostate cancer in Japan: possible protective effect of traditional Japanese diet. Cancer Sci. 2004;95:238–42.
24. Allen NE, Sauvaget C, Roddam AW, Appleby P, Nagano J, Suzuki G, Key TJ, Koyama K. A prospective study of diet and prostate cancer in Japanese men. Cancer Causes Control. 2004;15:911–20.
25. Xiang H, Schevzov G, Gunning P, Williams HM, Silink M. A comparative study of growth-inhibitory effects of isoflavones and their metabolites on human breast and prostate cancer cell lines. Nutr Cancer. 2002;42:224–32.
26. Davis JN, Singh B, Bhuiyan M, Sarkar FH. Genistein-induced upregulation of p21WAF1, downregulation of cyclin B, and induction of apoptosis in prostate cancer cells. Nutr Cancer. 1998;32:123–31.
27. Zhou JR, Yu L, Zhong Y, Nassr RL, Franke AA, Gaston SM, Blackburn GL. Inhibition of orthotopic growth and metastasis of androgen-sensitive human prostate tumors in mice by bioactive soybean components. Prostate. 2002;53:143–53.
28. Shen JC, Klein RD, Wei Q, Guan Y, Contois JH, Wang TT, Chang S, Hursting SD. Low-dose genistein induces cyclin-dependent kinase inhibitors and G(1) cell-cycle arrest in human prostate cancer cells. Mol Carcinog. 2000;29:92–102.
29. Hedlund TE, Johannes WU, Miller GJ. Soy isoflavonoid equol modulates the growth of benign and malignant prostatic epithelial cells in vitro. Prostate. 2003;54:68–78.
30. Shukla S, Gupta S. Molecular mechanisms for apigenin-induced cell-cycle arrest and apoptosis of hormone refractory human prostate carcinoma DU145 cells. Mol Carcinog. 2004;39:114–26.
31. Dalais FS, Meliala A, Wattanapenpaiboon N, Frydenberg M, Suter DA, Thomson WK, Wahlqvist M. Effects of a diet rich in phytoestrogens on prostate-specific antigen and sex hormones in men diagnosed with prostate cancer. Urology. 2004;64:510–5.
32. Kayisli UA, Aksu CA, Berkkanoglu M, Arici A. Estrogenicity of isoflavones on human endometrial stromal and glandular cells. J Clin Endocrinol Metab. 2002;87:5539–44.
33. Unfer V, Casini ML, Costabile L, Mignosa M, Gerli S, Di Renzo GC. Endometrial effects of long-term treatment with phytoestrogens: a randomized, double-blind, placebo-controlled study. Fertil Steril. 2004; 82:145–8.
34. Food Safety Commission [homepage on the Internet]. Tokyo: Basic concept of safety assessment on food for specified health uses including soybean isoflavone (in Japanese); [cited 2006 May]. Available from: http://www.fsc.go.jp/english/brochure/brochure2007/fsc07_p8.pdf
35. MacLean CH, Newberry SJ, Mojica WA, Khanna P, Issa AM, Suttorp MJ, Lim YW, Traina SB, Hilton L, et al. Effects of omega-3 fatty acids on cancer risk: a systematic review. JAMA. 2006;295:403–15.
36. Kagawa Y. Standard tables of food composition in Japan. 5th revised and enlarged ed. Tokyo: Kagawa Nutrition University; 2005
37. Etminan M, Takkouche B, Caamano-Isorna F. The role of tomato products and lycopene in the prevention of prostate cancer: a meta-analysis of observational studies. Cancer Epidemiol Biomarkers Prev. 2004;13:340–5.
38. Weinstein SJ, Wright ME, Pietinen P, King I, Tan C, Taylor PR, Virtamo J, Albanes D. Serum alpha-tocopherol and gamma-tocopherol in relation to prostate cancer risk in a prospective study. J Natl Cancer Inst. 2005;97:396–9.
39. Schuurman AG, Goldbohm RA, Brants HA, van den Brandt PA. A prospective cohort study on intake of retinol, vitamins C and E, and carotenoids and prostate cancer risk (Netherlands). Cancer Causes Control. 2002;13:573–82.
40. Goodman GE, Schaffer S, Omenn GS, Chen C, King I. The association between lung and prostate cancer risk, and serum micronutrients: results and lessons learned from beta-carotene and retinol efficacy trial. Cancer Epidemiol Biomarkers Prev. 2003;12:518–26.
41. Gann PH, Ma J, Giovannucci E, Willett W, Sacks FM, Hennekens CH, Stampfer MJ. Lower prostate cancer risk in men with elevated plasma lycopene levels: results of a prospective analysis. Cancer Res. 1999;59: 1225–30.
42. Helzlsouer KJ, Huang HY, Alberg AJ, Hoffman S, Burke A, Norkus FP, Morris JS, Comstock GW. Association between alpha-tocopherol, gamma-tocopherol, selenium, and subsequent prostate cancer. J Natl Cancer Inst. 2000;92:2018–23.
43. Li H, Stampfer MJ, Giovannucci EL, Morris JS, Willett WC, Gaziano JM, Ma J. A prospective study of plasma selenium levels and prostate cancer risk. J Natl Cancer Inst. 2004;96:696–703.
44. Vogt TM, Ziegler RG, Graubard BI, Swanson CA, Greenberg RS, Schoenberg JB, Swanson GM, Hayes RB, Mayne ST. Serum selenium and risk of prostate cancer in U.S. blacks and whites. Int J Cancer. 2003;103:664–70.

Original Research

Usefulness of Apparent Diffusion Coefficient Map in Diagnosing Prostate Carcinoma: Correlation with Stepwise Histopathology

Kengo Yoshimitsu, MD,[1]* Keijiro Kiyoshima, MD,[2] Hiroyuki Irie, MD,[1] Tsuyoshi Tajima, MD,[1] Yoshiki Asayama, MD,[1] Masakazu Hirakawa, MD,[1] Kousei Ishigami, MD,[1] Seiji Naito, MD,[3] and Hiroshi Honda, MD[1]

Purpose: To elucidate the performance of apparent diffusion coefficient (ADC) map in localizing prostate carcinoma (PC) using stepwise histopathology as a reference.

Materials and Methods: Preoperative MR images of 37 patients with PC who had undergone radical prostatectomy were retrospectively evaluated. First, T2-weighted images (T2WI) alone were interpreted (T2WI reading), and then T2WI along with ADC map were interpreted (T2WI/ADC map reading). Sextant-based sensitivity and specificity, and the ratio of the detected volume to the whole tumor volume (% tumor volume) were compared between the two interpretations, and results were also correlated to Gleason's scores (GS). ADC values were correlated to histological grades.

Results: Sensitivity was significantly higher in T2WI/ADC map reading than in T2WI reading (71% vs. 51%), but specificity was similar (61% vs. 60%). By adding ADC map to T2WI, % tumor volume detected increased significantly in transitional zone (TZ) lesions, but not in peripheral zone (PZ) lesions. % tumor volume detected with T2WI/ADC map reading showed a positive correlation with GS of the specimens. Less differentiated PC were associated with lower ADC values and higher detectability.

Conclusion: T2WI/ADC map reading was better than T2WI reading in PC detection and localization. This approach may be particularly useful for detecting TZ lesions and biologically aggressive lesions.

Key Words: prostate carcinoma; MR; diffusion-weighted image; ADC map; localization
J. Magn. Reson. Imaging 2008;27:132–139.

PROSTATE CARCINOMA (PC) is one of the most common malignancies in males, and it accounts for approximately 30,000 new annual deaths in the United States (1). To date, surgical resection of the whole organ has been the only method of eradicating this type of malignancy; however, less invasive alternative local therapies, including intensive modulated radiation therapy (IMRT), high-intensity focused ultrasound (HIFU), and brachytherapy, are being introduced due to the increasing clinical demand for the preservation of functional aspects of the prostate and related organs (2–4).

The current role of MRI in the diagnosis of PC is primarily based on T2-weighted images (T2WI), and this approach has remained relatively limited in terms of usefulness, as it can mainly be used to determine whether or not a lesion extends beyond the confinement of the organ capsule (5), a measure used for determining the indication for radical prostatectomy. Also, in the cases of the less invasive local therapies mentioned above, the current approach is to cover the whole organ, regardless of the location or bulk of the tumor within the organ, provided extracapsular extension of the tumor has been excluded (2–4). Because PC can be multifocal and involve any part of the organ, more precise localization and focal targeting of lesions may be beneficial for patients, potentially rendering retreatment for the recurrent tumors possible, in addition to maximizing the options for the preservation of function.

Various MR approaches have been investigated and applied to localize PC; such attempts have included dynamic studies and MR spectroscopy, which provided promising but inconsistent results (6–16). Diffusion-weighted images (DWI) and calculated apparent diffusion coefficient (ADC) mapping are additional approaches, involving the representation of the Brownian movement of water molecules. This new parameter dif-

[1]Department of Clinical Radiology, Graduate School of Clinical Sciences, Kyushu University, Fukuoka, Japan.
[2]Department of Anatomic Pathology, Graduate School of Clinical Sciences, Kyushu University, Fukuoka, Japan.
[3]Department of Urology, Graduate School of Clinical Sciences, Kyushu University, Fukuoka, Japan.
*Address reprint requests to: K.Y., Department of Clinical Radiology, Graduate School of Medical Sciences, Kyushu University, 3-1-1, Maidashi, Higashi-ku, Fukuoka, 812-8582, Japan.
E-mail kengo@med.kyushu-u.ac.jp
Received December 31, 2006; Accepted August 29, 2007.
DOI 10.1002/jmri.21181
Published online in Wiley InterScience (www.interscience.wiley.com).

fers from conventional T1 or T2 relaxivity, dynamic enhancement characteristics, or spectroscopic information. This DWI or the ADC map has been applied for examining various part of the body, in particular to detect or differentiate malignancies (17–20). Regarding PC, several preliminary investigations have been sporadically reported (21–25), with promising results. In this article, we applied the ADC map obtained from DWI to the diagnosis of PC, and evaluated its performance at detecting and localizing PC using stepwise histopathological data as a gold standard. We also correlated the results to the histological grades of the lesions and Gleason's scores (GS) of the specimens, in order to characterize the potential clinical usefulness of this novel technique.

MATERIALS AND METHODS

Patients

Between January 2000 and March 2004, 124 patients underwent radical prostatectomy at our institute. Among these patients, 37 who had undergone preoperative MRI (including DW imaging) were retrospectively selected, and these 37 patients formed the present study population. One of the 37 subjects had received hormonal therapy prior to surgery. The age of the selected patients ranged from 56 to 75 years old (mean = 66 years). The preoperative prostate-specific antigen (PSA) level ranged from 0.7 to 54.8 ng/mL, with a mean of 11.9 (normal range < 4.00 ng/mL). All subjects had undergone transrectal or transperineal biopsy prior to MR imaging and had been pathologically diagnosed with malignant foci in the prostate. The period between biopsy and MR ranged from six to nine weeks (mean = 7.2 weeks), and the period between MR and surgery ranged from zero to eight weeks (mean = 2.5 weeks). The institutional review board at our hospital did not require that written informed consent be obtained for this study due to its retrospective nature. The current study was designed and performed according to the declaration of Helsinki (26).

MR Equipment and Parameters

A total of two 1.5T units (Magnetom Symphony and Vision; Siemens, Erlangen, Germany) were used with a pelvic multichannel phased-array coil (12 channels). After routine T1-weighted spin-echo (TR/TE/number of excitations [NEX] = 500 msec/12 msec/2) axial images had been obtained, T2-weighted fast spin-echo (TR/TE/Turbo factor/NEX = 3000 msec/102 msec/15/3, slice thickness = 5 mm, interslice gap = 30%) axial and coronal images with axial DWI were obtained using the single-shot spin-echo echo-planar imaging (EPI) technique. The matrix and field-of-view of the T1- and T2-weighted images (T1WI and T2WI) were 256 × 512, and 20 cm, respectively. The slice thickness and gap of DWI were identical to those of routine T1WI and T2WI. Sequential sampling of the k-space was used with echo-time (TE) = 110–135 msec and bandwidth = 1250 Hz/pixel, and 128 lines of data were acquired in 0.3 seconds. No parallel imaging technique was applied. Other parameters included a field-of-view = 240 mm, matrix size = 128 × 128, and the acquisition of four signals. All images were obtained while the patients maintained normal and consistent breathing, and a fat-saturated pulse was used for the DWI to exclude severe chemical-shift artifacts. A contrast-enhanced dynamic study was performed and postcontrast T1WI were obtained in all cases, the details of which are not given here, as they are out of the scope of this work.

DWI were acquired with motion-probing gradient pulses applied along three (x-, y-, and z-axes) directions with three b factors of 0, 500, and 1000 seconds/mm^2. ADC maps were automatically generated on the operating console using all seven images (b = 0 and two b-values in each direction), and the ADC values were obtained by measuring the intensity of the map.

Pathological Map Preparation

One experienced pathologist created transverse sections of the specimens: the most apical and basic sides of the specimen were cut to a thickness of 6 mm, and the remaining portion (majority of the specimen) were cut to a thickness of 4 mm. Each section of each specimen was digitally photographed together with a ruler along the edge, which serve as a size reference, and the areas of the PC that had been microscopically determined were marked on the digital photographs by the pathologist (pathological map) using commercially available presentation software (Microsoft PowerPoint 2002; Microsoft Corporation, Redmond, WA, USA). All PC foci, including infiltrating foci that did not form apparent masses, were marked on the map and divided into the sextants according to their location, as follows: right and left apices (lower third), midglands (middle third), and bases (upper third). Lesions consisting of uniform histological grades were also documented as such on the photograph. This pathological map was used as the gold standard in this study.

Assessment

First, we subdivided the glands of all patients into sextants on the MR images. The presence of PC in each sextant was retrospectively evaluated and recorded by two radiologists in a consensus. Initially, T2WI alone (T2WI reading) were interpreted and then T2WI and the ADC map (T2WI/ADC map reading) were interpreted. The readers were informed that the patients had undergone surgery for PC, but no other clinical information, (e.g., PSA level or biopsy results) was provided to the readers. On either T2WI or the ADC map, areas with apparently lower signal intensity than that of the surrounding tissue were considered to represent PC, according to the previously reported descriptions (5–16,21–25). Regarding T2WI/ADC map reading, when the findings on either sequence were equivocal, those on the ADC map were considered to have priority, if image degradation is not prominent. Sensitivity and specificity were thus calculated based on the sextant evaluation and the results of the two interpretations were compared.

We then directly compared the MR images and the pathological map on a lesion basis, and we excluded

positive sextants in which the noncancerous areas had been interpreted as PC on the MR images (false-positive lesions in positive sextants); thus the true sensitivity was calculated. As for a lesion whose location at least partially overlapped on the MR images and on the pathological map, the lesion was considered false-positive when the maximum transverse diameter measured at MRI was out of the range of 50% to 150% of the maximum transverse diameter measured on the pathological map (16). Lesions seen at MRI were only considered truly positive if the suspected foci were in the same relative portion of the prostate.

We also marked the approximate areas of PC on a pathological map, which had been detected on MR images (detected PC) using MR images as reference, and the areas of the whole PC and the detected PC were traced and measured using NIH software (NIH Image, version 1.63; National Institutes of Health, Bethesda, MD, USA). Volume was calculated by multiplying the measured areas by thickness (0.4 cm). False-positive lesions, including those in positive sextants as defined above, were excluded in this evaluation. Thus, % tumor volume (percentage of the tumor volume detected to the whole tumor volume; range = 0–100%) per patient was compared between the T2WI reading and T2WI/ADC map reading. The lesions were subclassified into peripheral zone (PZ) and transitional zone (TZ) lesions according to their location on the pathological map, and these two groups were compared in terms of % tumor volume per patient. Then, the % tumor volume per patient was also correlated to the GS of the patients.

Lesions with uniform histological grades that were larger than 1 cm in their short axes were selected on the pathological map and their ADC values were measured at the corresponding sites on the ADC map by one radiologist, even when there were no detectable abnormal areas on the ADC map. Correlation of ADC value and histological grades was thus evaluated. We also evaluated the detectability of these lesions in correlation with the their histological grades.

Finally, by comparing the MR images and pathological maps, we selected areas of PC larger than 1 cm in their short axes that had not been detected on ADC map (false-negative lesions). The possible reasons for these lesions not being detected on MR images were analyzed. We also selected areas of low signal intensity larger than 1 cm in their short axes on the ADC map that did not correspond to PC on the pathological map (false-positive lesions). The corresponding sites were marked on the pathological map, and pathological details of these areas were then reevaluated by the pathologist.

RESULTS

In one patient, microscopic evaluation of the resected gland revealed no PC, although preoperative biopsy had suggested the presence of PC in one of the sextants. A total of 222 sextants in 37 patients were evaluated, among which 147 sextants were positive and 75 were negative for the presence of PC. A total of 79 and 105 positive sextants, and 45 and 46 negative sextants were correctly diagnosed with T2WI reading and T2WI/ADC map reading, respectively. Among the 79 and 105 positive sextants that were classified as positive, 45 and 31 were excluded for the calculation of true sensitivity because they were regarded as noncancerous areas on the lesion-based evaluation. The sensitivity, true sensitivity, and specificity of T2WI reading were 53%, 23%, and 60%, whereas the sensitivity, true sensitivity, and specificity of the T2WI/ADC map reading were 71%, 50%, and 61%, respectively. There was a significant difference between the two interpretations in terms of the sensitivity and true sensitivity ($P < 0.01$, McNemar chi-squared test), but no difference in the specificity ($P = 0.97$).

The areas of PC on the pathological map ranged from 3 mm to 22 mm in their shortest dimension (mean = 7 mm). The calculated volumes of PC per patient ranged from 0 to 5.75 cm^3 (mean = 1.49 cm^3). There were 261 and 151 areas of the PC in PZ and TZ; the sum of tumor volume were 38.8 and 16.3 cm^3, respectively. The majority (33/37) of our patients had areas of PC in both PZ and TZ. The mean % tumor volume per patient detected by T2WI reading were 20% (range = 0–100%), 41% (range = 0–100%), and 7% (range = 0–91%), for total lesions, the PZ lesions, and TZ lesions, respectively. The mean % tumor volume per patient detected by T2WI/ADC map reading for total lesions, the PZ lesions, and TZ lesions, were 47% (range = 0–100%), 48% (range = 0–100%), and 44% (range = 0–100%), respectively. Overall (not per patient, but total sum) % tumor volume by T2WI reading were 30%, 55%, and 20%, for total lesions, the PZ lesions, and TZ lesions, respectively. Overall % tumor volume by T2WI/ADC map for total lesions, the PZ lesions, and TZ lesions, reading were 55%, 57%, and 52%, respectively. Addition of the ADC map to T2WI interpretation revealed a significant increase in % tumor volume in total lesions ($P = 0.0002$, Wilcoxon signed rank test) and in TZ lesions ($P < 0.0001$), but not in PZ lesions ($P = 0.158$, not significant [NS]).

For the resected specimens in 35 patients (excluding one patient whose specimen revealed no evidence of PC and another who had received hormonal therapy), GS were assigned. There was a weak but significant correlation between % tumor volume by T2WI/ADC map reading and GS ($\rho = 0.40$, $P = 0.022$, Spearman's rank correlation test) (Fig. 1). Patients with higher GS tended to have higher % tumor volume, namely had more chance for PC to be detected by T2WI/ADC map reading. No significant correlation was observed between % tumor volume detected by T2WI reading alone and GS ($P = 0.41$, NS). Because it has been reported that the larger the tumor is, there is the better correlation between tumor volume measured on T2WI and histopathologic volume (14), we might need to exclude the effect of the volume of PC in evaluating the correlation between % tumor volume by T2WI/ADC map reading and GS. We therefore evaluated the partial correlation coefficient between either tumor volume or GS and % tumor volume detected (Table 1). The results showed that % tumor volume detected with T2WI/ADC map reading significantly correlated to GS, but not to tumor volume, and also that % tumor volume detected with T2WI reading correlated to the tumor volume, but not to GS.

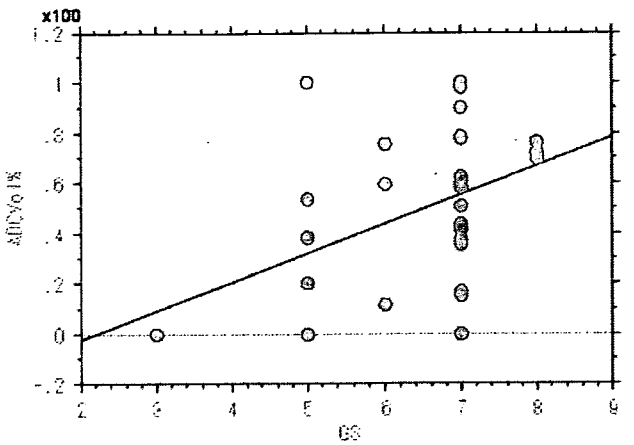

Figure 1. Correlation between % tumor volume detected by T2WI and ADC map interpretation and GS of the specimens. There was a weak but significant correlation (ρ = 0.40, P = 0.022, Spearman's rank correlation test). ADC Vol% = % tumor volume detected with T2WI and ADC map interpretation, GS = Gleason's scores.

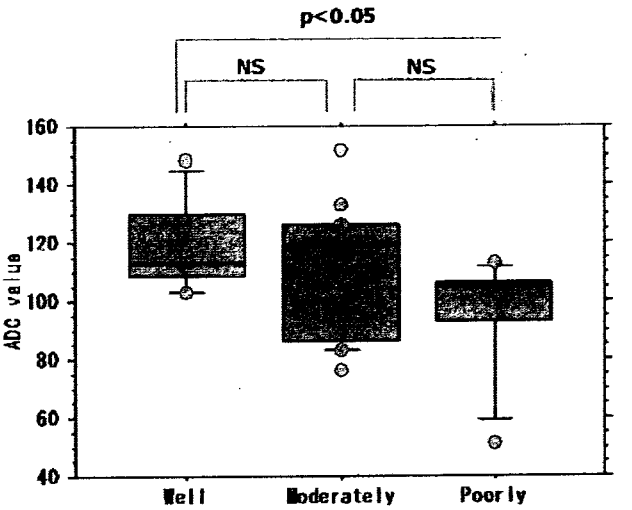

Figure 2. Correlation between ADC values and histological grades of PC. ADC values of well-, moderately-, and poorly-differentiated adenocarcinoma were 1.19 ± 0.15, 1.10 ± 0.24, and 0.93 ± 0.20 × 10^{-3} mm^2/second (mean ± SD), respectively. Difference was significant only between well- and poorly-differentiated carcinoma (P = 0.019, one-way factorial ANOVA with Scheffe's post-hoc test). There was a subtle, but significant correlation (Spearman's rank correlation test, ρ = −0.144, P = 0.045). A horizontal line in the middle of each box indicates a median of each group. [Color figure can be viewed in the online issue, which is available at www.interscience.wiley.com.]

Regarding the ADC value measurement, 53 lesions with uniform histological grades that were larger than 1 cm in their short axes were selected from 36 patients. There were 21, 26, and six lesions, in well-, moderately-, and poorly-differentiated adenocarcinomas, respectively. The mean size (short axis diameter) of these lesions was 1.14 cm (range: 1.0–1.9 cm), 1.23 cm (1.0–2.2 cm), and 1.03 cm (1.0–1.2), respectively, showing no significant difference (P = 0.38, one-way factorial analysis of variance [ANOVA]). The ADC values of well-, moderately-, and poorly-differentiated PC were 1.19 ± 0.15, 1.10 ± 0.24, and 0.93 ± 0.20 × 10^{-3} mm^2/second (mean ± standard deviation [SD]), respectively. Significant difference in ADC values was seen only between well- and poorly-differentiated PC (P = 0.019), and difference between well- and moderately-differentiated, or that between moderately- and poorly-differentiated PC was not significant (P = 0.38 and 0.13, one-way factorial ANOVA with Scheffe's post hoc test). There was a subtle but significant correlation between the histological grades and ADC values (ρ = −0.18, P = 0.014, Spearman's rank correlation) (Fig. 2). Of these 53 lesions, 13 (62%), 24 (92%), and six (100%) were detected on the ADC map, in well-, moderately-, and poorly-differentiated adenocarcinomas, respectively. The detectability of these lesions differed significantly among histological grades (Kruskal-Wallis test, P < 0.01) and a significant correlation was observed, whereby the less differentiated lesions were associated with higher detectability (P < 0.01, Cochran-Armitage test for trend).

As for false-positive lesions, 54 foci were selected from 27 patients. The pathological details of these lesions included hyperplastic nodules in 22, normal structure in 14 (periejaculatory duct tissue in five, asymmetric central zone tissue in four, base of the seminal vesicle in three, asymmetric anterior fibromuscular stroma in one, and vermontanum in one), intraacinar hemorrhage in 10, and chronic prostatitis in eight. As for false-negative lesions, 15 foci in 15 patients were selected. Possible causes for these false-negatives were well-differentiated infiltrative lesions with preserved gland formation in six lesions, susceptibility artifact from rectal or intestinal gas in four lesions, and susceptibility artifact from metallic prosthesis at the hip joint in one lesion. Causes for the remaining four lesions remained unknown. Representative cases are shown in Figs. 3, 4, and 5.

Table 1
Partial Correlation Coefficient Based on Spearman's Rank Correlation Coefficient Between Either Tumor Volume or Gleason's Score and % Tumor Volume Detected by T2WI Reading Alone and T2WI/ADC Map Reading

	% Tumor volume detected	
	T2WI	T2WI/ADC map
Tumor volume		
Partial ρ	0.4439	0.045
P-value	0.0109	0.8065
Gleason's score		
Partial ρ	−0.0535	0.3507
P-value	0.7712	0.0491

T2WI = T2-weighted image reading, T2WI/ADC map = T2-weighted image and apparent diffusion coefficient map reading, ρ = correlation coefficient.

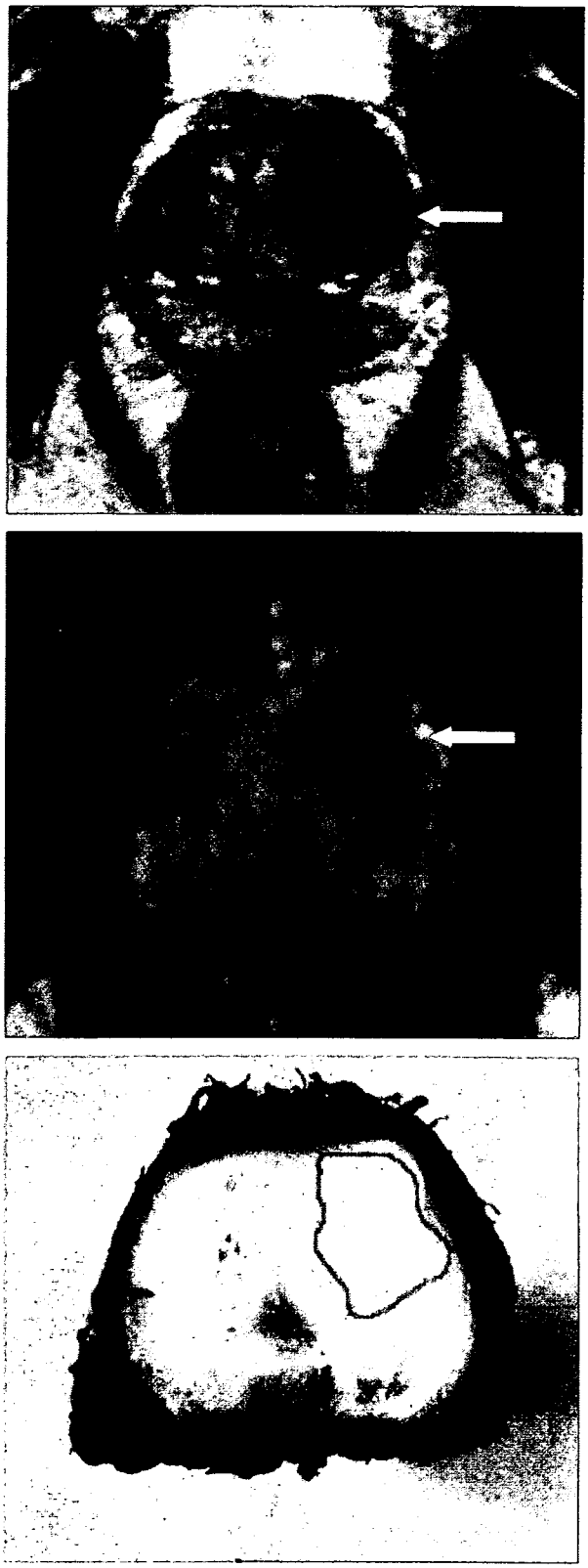

Figure 3. A 69-year-old man with a preoperative PSA level of 12.5 ng/mL. There was a moderately differentiated adenocarcinoma at the left TZ (GS: 3 + 5 = 8) confined within the gland. Both T2WI (**a**) and ADC map (**b**) clearly demonstrated carcinoma as low signal intensity areas (arrows). An encircled area represents the carcinoma on the pathological map (**c**). [Color figure can be viewed in the online issue, which is available at www.interscience.wiley.com.]

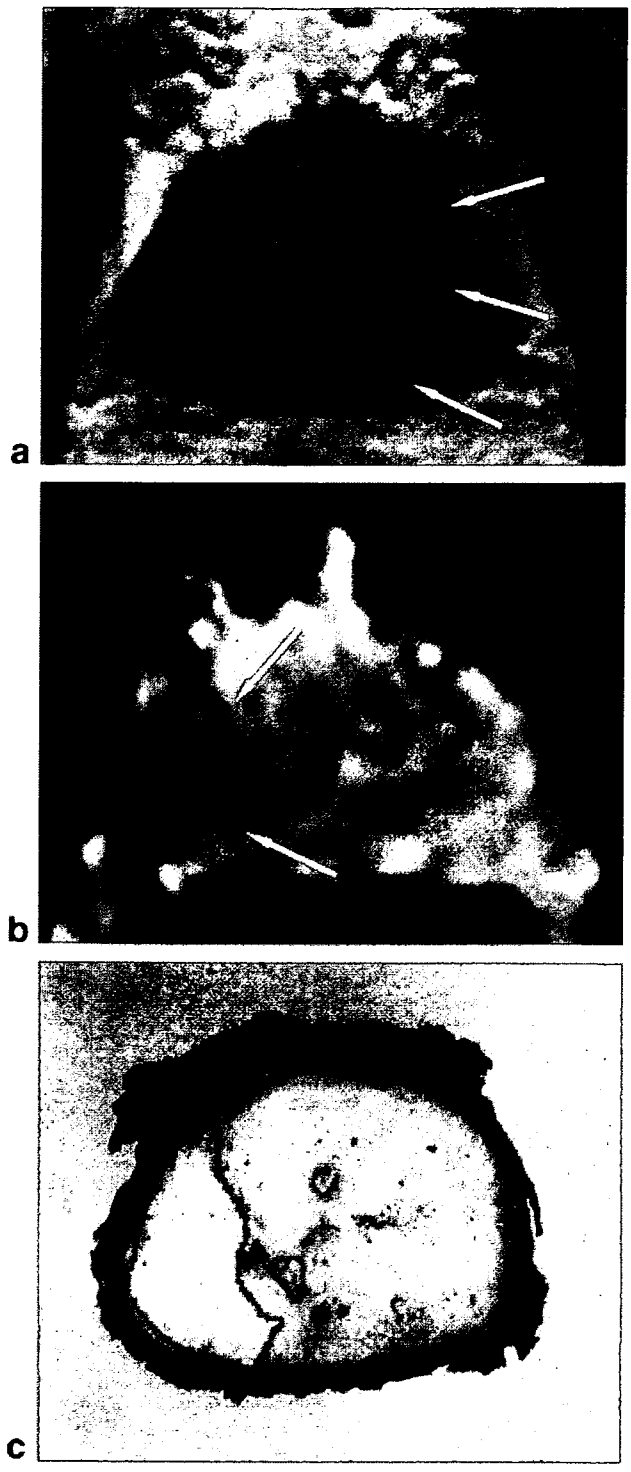

Figure 4. A 63-year-old male with an initial PSA level of 16 ng/mL. The patient received hormonal therapy using chrormadinone acetate and leuprorelin acetate for three months and the PSA level decreased to 0.8 ng/mL just before surgery. There was a moderately- to poorly-differentiated adenocarcinoma at the right PZ, confined within the gland. GS was not evaluated because of cellular degeneration. On T2WI (**a**), approximately two-thirds of the gland on the right exhibited low signal intensity (arrows). On ADC map (**b**), an area of low signal was localized at the right PZ (arrows), which corresponded well to the area of carcinoma shown on the pathological map (**c**) (encircled areas). [Color figure can be viewed in the online issue, which is available at www.interscience.wiley.com.]

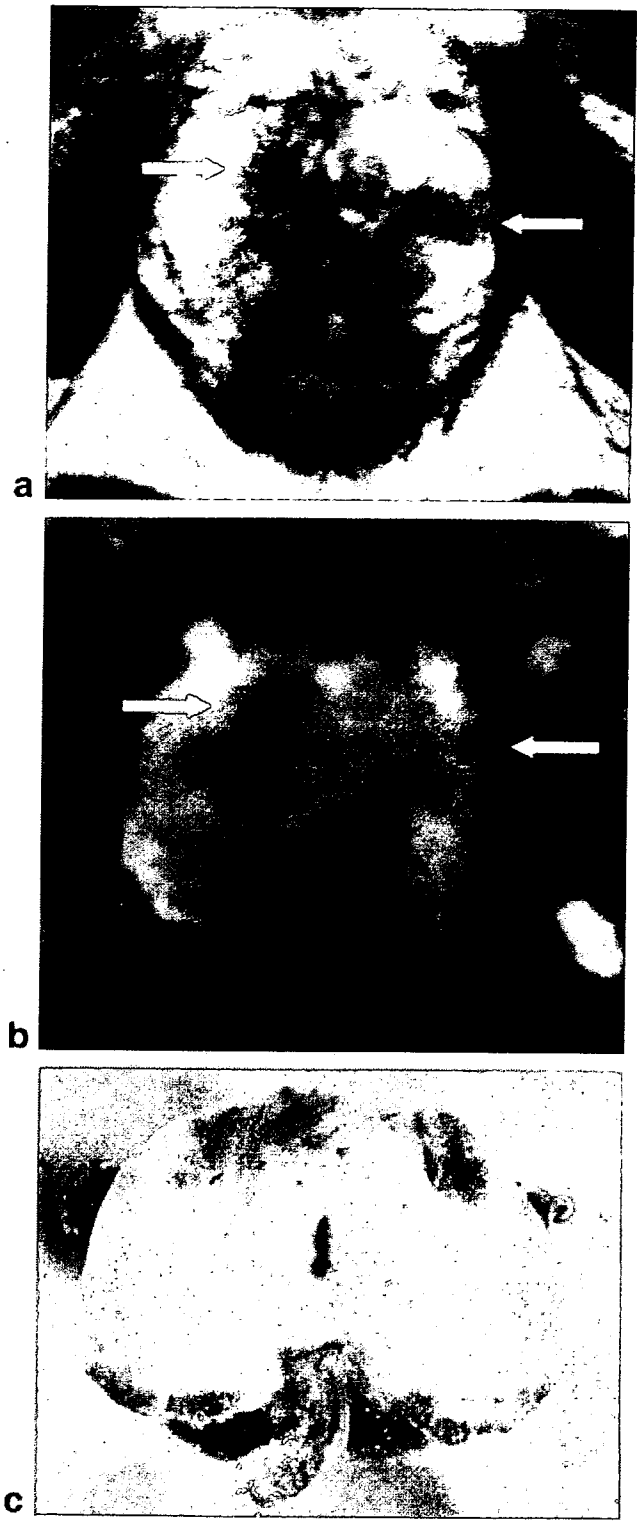

Figure 5. A 59-year-old male with a preoperative PSA level of 0.7 ng/mL and positive biopsy results. There was a small focus (3 mm in diameter) of well-differentiated adenocarcinoma at the apex of the gland (not shown), with a GS of 3 + 2 = 5. The major portion of the gland was free of carcinoma cells. There were several areas of low signal intensity, both on T2WI (**a**) and ADC map (**b**) (arrows); however, there was no carcinoma at the corresponding sites on the pathological map (**c**). Hyperplastic glandular and interstitial cells were noted at theses sites upon reevaluation of the specimen. [Color figure can be viewed in the online issue, which is available at www.interscience.wiley.com.]

DISCUSSION

Previous investigators have reported significant difference in ADC values between PC and normal prostatic tissue, using biopsy-proven histopathology as a reference (21–25). To date, there have been few reports regarding PC detection with DWI or ADC mapping in patients who had undergone prostatectomy. We therefore attempted in the present study to clarify the clinical usefulness and significance of DWI or ADC mapping using a stepwise histopathology as a gold standard.

According to our results, sextant-based sensitivity and true sensitivity improved significantly, i.e., up to 71% and 50%, respectively, when the ADC map was interpreted along with T2WI, although the specificity remained unchanged at around 60%. In terms of the volume of PC, T2WI/ADC map reading detected approximately one-half of the tumor in the gland. Previously reported sensitivity and/or detection rate of PC on MRI (i.e., T2WI with or without spectroscopy), has been in a range between 20% to 80% (6–16). Recently, Hom et al (16) reported a detection rate of around 20% using endorectal coil MR images and MR spectroscopy for cases of PC in PZ, and using meticulous histopathologic evaluation methods and strict criteria. Our data also revealed a rather low sensitivity or detection rate, at least in part because we also used the pathological map as a strict gold standard, including all small foci of PC. Another explanation for this low sensitivity may have been the criteria we used to detect PC in our study. Namely, we considered "areas with low signal intensity relative to the surrounding tissue" as PC in both PZ and TZ; however, Li et al (27) recently applied more meticulous criteria to diagnose TZ lesions and achieved better results. Although the application of different criteria might have improved the sensitivity, our present data suggest that a T2WI/ADC map reading cannot be used as a reasonable guide yet in localization of PC in the context of local therapies such as IMRT or HIFU. Practical use of ADC maps may therefore be limited at present, for example, to a guide for rebiopsy in patients with high PSA levels but with negative biopsy results.

To improve sensitivity of the T2WI/ADC map reading, it will be necessary to detect well-differentiated PC with glandular formation, which was the most common cause of false negativity in our series. In our evaluation of the lesions larger than 1 cm in the shortest dimension, the ADC values of well-differentiated PC were significantly higher than moderately- or poorly-differentiated PC, and nearly one-half of these lesions were visually missed on the T2WI/ADC map interpretation. The pathological architecture of these lesions, namely, preserved glandular formation with a significant volume of fluid-filled luminal space, which is similar to that of normal prostatic glandular tissue, supports the relatively high ADC values of these lesions; these features rendered it difficult to detect such lesions on the ADC map. Improving the signal-to-noise ratio (SNR) by using 3T hardware or a coil with more channels may help detect these lesions. Concurrent usage of a parallel imaging technique (24,28,29) may also help reduce the susceptibility artifacts, the second most common cause of false negativity.

To improve specificity, it will be necessary to differentiate between hyperplastic nodules and PC; the lack of such differentiation was the most common cause of false positivity in our results. Again, improving the SNR by either the use of 3T hardware or new coils may help differentiate these two entities. The second most common reason for false positivity was normal prostatic tissue, including periejaculatory duct tissue, central zone tissue, tissue at the base of the seminal vesicle, and so on. The ADC values of these structures were $0.97 \pm 0.18 \times 10^{-3}$ mm^2/second (not shown in the results), which were within the range of ADC values of PC. Precise anatomic evaluation may obviate this misdiagnosis; however, it would remain difficult to discriminate these structures from focal involvement of PC on an ADC map. Combination with MR spectroscopy or dynamic MR study may be of some help in resolving this problem.

The promising aspects of our findings are as follows. First, the T2WI/ADC map reading significantly increased the detection of PC located in TZ. In terms of the % tumor volume, the detection rate of T2WI/ADC map reading was approximately 50% regardless of the location of PC, whereas that of T2WI reading alone was significantly worse in the case of lesions in TZ than in those in PZ. Because PC in TZ has remained a diagnostic problem either for transrectal ultrasound (US) or conventional MR, use of DWI and ADC maps could be of aid in the detection of lesions in TZ in particular. Although Li et al (27) recently reported improved detection of PC in TZ using the combined criteria of T2WI and postcontrast T1WI, adding information of ADC map might further improve the detection of PC in TZ.

A second promising point suggested by our results was that the higher the histological grade of PC, the lower the ADC values of PC, which increases the chances of PC being detected on an ADC map. This finding may also be related to the positive correlation between % tumor volume detected by T2WI/ADC map reading and GS (Table 1). Such information may be clinically important because it may suggest that the biologically aggressive components or subsets of PC are more likely to be detected by T2WI/ADC map reading than would less aggressive components. As the histological grade or GS increases, there have been shown to be more chances of cellular architectures exhibiting little gland formation, such as medullary or solid patterns (30,31); these features may explain the low ADC values in these lesions. Although the ADC values obtained in our study were comparable to the previously reported values (21–25), this is the first study to reveal the relationship between histological grade or GS and ADC values in cases of PC.

A third promising issue suggested by the results from but a single patient was that the areas of PC was relatively clearly depicted on ADC map within areas of diffusely decreased signal intensity on T2WI; this was a patient who had received preoperative hormonal therapy (androgen deprivation) (Fig. 4). It was already well known that posthormonotherapy prostatic tissue becomes atrophic and diffusely hypointense, which impairs pertinent MR detection of PC (32,33). The ADC map might be of help in evaluating patients still undergoing or following hormonal therapy.

There are several limitations to the present study. First, this study was retrospective in nature, and all patients in this series had undergone biopsy prior to MR examination. Although the period between biopsy and MR examination in our study was more than one month, which is reportedly sufficient to avoid biopsy effects on MR images (34,35), the histopathological evaluation revealed intraacinar hemorrhage, which was the third most common cause of false positivity. Another technical aspect related to the retrospective nature of the study was the subtle differences between MR images and pathological section in terms of the slice interval and slice direction; such differences might have exerted an influence on the precise correlation between the depicted abnormality and the lesions observed on the pathological map. Prospective studies are needed that are designed in such a manner that MR examination is performed prior to biopsy and in which the MR and pathological sections are identical. In addition, due to the limitation associated with the hardware, TE of EPI used for the DWI was rather long (110–135 msec) in our study, as compared to that of previous reports (96–120 msec) (21–25). This long TE may have led to the low SNR of the images, particularly in cases involving tissues with short T2 characteristics, which in turn possibly led to the incorrect calculation of ADC values. Use of a parallel imaging technique might have improved this situation, allowing for a shorter TE (24,28,29), although this technique was not available at the time we started this study. Third, because of the significant image distortion of the ADC map, we did not perform any volume measurement on MR images, although in this study, such measurements were carried out on the pathological map by encircling the approximate area of PC by visual inspection using MR images as a reference. Again, a parallel imaging technique would have been useful to reduce the image distortion secondary to the susceptibility effect from intestinal gas or metallic prosthesis (24,28,29), which would in turn have enabled us to measure the areas of interest on the ADC map.

In conclusion, the ADC map derived from DWI of MRI performed with a phased array coil without parallel imaging technique significantly improved PC detection and localization when interpreted together with T2WI, although the performance of this method might not yet be sufficient for it to serve as a guide for local therapies. This novel approach to the diagnosis of PC is expected to be particularly useful for the detection of PC lesions located in TZ, as well as detection of lesions with relatively little differentiation, and lesions with a relatively high GS.

ACKNOWLEDGMENT

We thank Professor Masasumi Tsuneyoshi, Chair of the Department of Anatomic Pathology, Graduate School of Medical Sciences, Kyushu University, for providing us pathologic specimens for this study.

REFERENCES

1. American Cancer Society. Cancer Facts and Figures 2004. Atlanta, GA: American Cancer Society; 2004. 60 p. Available at: http://www.cancer.org/downloads/STT/CAFF_finalPWSecured.pdf. Last accessed: September 20, 2007.
2. Carroll PR, Presti JC Jr, Small E, Roach M III. Focal therapy for prostate cancer 1996: maximizing outcome. Urology 1997; 49(Suppl 3A):84–94.
3. Meerleer GD, Villeirs G, Bral S, et al. The magnetic resonance detected intraprostatic lesions in prostate cancer: planning and delivery of intensity-modulated radiotherapy. Radiother Oncol 2005;75:325–333.
4. Blana A, Walter B, Rogenhoer S, Wieland W. High-intensity focused ultrasound for the treatment of localized prostate cancer: 5-year experience. Urology 2004;63:297–300.
5. Rajesh A, Coakley FV. MR imaging and MR spectroscopic imaging of prostate cancer. Magn Reson Imaging Clin N Am 2004;12:557–579.
6. Engelbrecht MR, Huisman HJ, Laheij RJ, et al. Discrimination of prostate cancer from normal peripheral zone and central gland tissue by using dynamic contrast-enhanced MR imaging. Radiology 2003;229:248–254.
7. Hasumi M, Suzuki K, Taketomi A, et al. The combination of multivoxel MR spectroscopy with MR imaging improve the diagnostic accuracy for localization of prostate cancer. Anticancer Res 2003; 23:4223–4227.
8. Ikonen S, Kivisaari L, Tervahartiala P, Vehmas T, Taari K, Rannikko S. Prostatic MR imaging. Accuracy in differentiating cancer from other prostatic disorders. Acta Radiol 2001;42:348–354.
9. Dhingsa R, Qayyum A, Coakley FV, et al. Prostate cancer localization with endorectal MR imaging and MR spectroscopic imaging: effect of clinical data on reader accuracy. Radiology 2004;230:215–220.
10. Kurhanewicz J, Swanson MG, Nelson SJ, Vigneron DB. Combined magnetic resonance imaging and spectroscopic imaging approach to molecular imaging of prostate cancer. J Magn Reson Imaging 2002;16:451–463.
11. Kumar R, Kumar M, Jagannathan NR, Gupta NP, Hemal AK. Proton magnetic resonance spectroscopy with a body coil in the diagnosis of carcinoma prostate. Urol Res 2004;32:36–40.
12. Kiessling F, Huber PE, Grobholz R, et al. Dynamic magnetic resonance tomography and proton magnetic resonance spectroscopy of prostate cancers in rats treated by radiotherapy. Invest Radiol 2004;39:34–44.
13. Kaji Y, Wada A, Imaoka I, et al. Proton two-dimensional chemical shift imaging for evaluation of prostate cancer: external surface coil vs. endorectal surface coil. J Magn Reson Imaging 2002;16:697–706.
14. Coakley FV, Kurhanewicz J, Lu Y, et al. Prostate cancer tumor volume: measurement with endorectal MR and MR spectroscopic imaging. Radiology 2002;223:91–97.
15. Purohit RS, Shinohara K, Meng MV, Carroll PR. Imaging clinically localized prostate cancer. Urol Clin North Am 2003;30:279–293.
16. Hom JF, Coakley FV, Simko JP, et al. Prostate cancer: endorectal MR imaging and MR spectroscopic imaging—distinction of true-positive from chance-detected lesions. Radiology 2006;238:192–199.
17. Ichikawa T, Haradome H, Hachiya J, Nitatori T, Araki T. Diffusion-weighted MR imaging with a single-shot echoplanar sequence: detection and characterization of focal hepatic lesions. AJR Am J Roentgenol 1998;170:397–402.
18. Castillo M, Smith JK, Kwock L, Wilber K. Apparent diffusion coefficients in the evaluation of high-grade cerebral gliomas. AJNR Am J Neuroradiol 2001;22:60–64.
19. Nakayama T, Yoshimitsu K, Irie H, et al. Usefulness of the calculated apparent diffusion coefficient value in the differential diagnosis of retroperitoneal masses. J Magn Reson Imaging 2004;20:735–742.
20. Nakayama T, Yoshimitsu K, Irie H, et al. Diffusion-weighted echoplanar MR imaging and ADC mapping in the differential diagnosis of ovarian cystic masses: usefulness of detecting keratinoid substances in mature cystic teratomas. J Magn Reson Imaging 2005; 22:271–278.
21. Gibbs P, Tozer DJ, Liney GP, Turnbull LW. Comparison of quantitative T2 mapping and diffusion-weighted imaging in the normal and pathologic prostate. Magn Reson Med 2001;46:1054–1058.
22. Issa B. In vivo measurement of the apparent diffusion coefficient in normal and malignant prostatic tissues using echo-planar imaging. J Magn Reson Imaging 2002;16:196–200.
23. Hosseinzadeh K, Schwarz SD. Endorectal diffusion-weighted imaging in prostate cancer to differentiate malignant and benign peripheral zone tissue. J Magn Reson Imaging 2004;20:654–661.
24. Sato C, Naganawa S, Nakamura T, et al. Differentiation of noncancerous tissue and cancer lesions by apparent diffusion coefficient values in transition and peripheral zones of the prostate. J Magn Reson Imaging 2005;21:258–262.
25. Shimousa R, Fujimoto H, Akamata H, et al. Diffusion-weighted imaging of prostate cancer. J Comput Assist Tomogr 2005;29:149–153.
26. World Medical Association. Declaration of Helsinki: ethical principles for medical research involving human subjects. Ferney-Voltaire, France: World Medical Association; 2004. 5p. Available at: http://www.wma.net/e/policy/b3.htm. Last accessed: September 20, 2007.
27. Li H, Sugimura K, Kaji Y, et al. Conventional MR capabilities in the diagnosis of prostate cancer in the transition zone. AJR Am J Roentgenol 2006;186:729–742.
28. Sodickson DK, McKenzie CA. A generalized approach to parallel magnetic resonance imaging. Med Phys 2001;28:1629–1643.
29. Jaermann T, Crelier G, Pruessmann KP, et al. SENSE-DTI at 3 T. Magn Reson Med 2004;51:230–236.
30. Gleason DF, Vacu RG. Histologic grading and clinical staging of prostatic carcinoma. In: Tannenbaum M, editor. Urologic pathology: the prostate. Philadelphia: Lea and Febiger; 1997. p 171–197.
31. Epstein JI. Urinary tract and male genital system. The prostate and seminal vesicle. In: Sternberg SS, editor. Diagnostic surgical pathology. New York: Raven Press; 1989. p 1393–1432.
32. Chen M, Hricak H, Kalbhen CL, et al. Hormonal ablation of prostatic cancer: effects on prostate morphology, tumor detection, and staging by endorectal coil MR imaging. AJR Am J Roentgenol 1996; 166:1157–1163.
33. Padhani AR, MacVicar AD, Gapinsli CJ, et al. Effects of androgen deprivation on prostatic morphology and vascular permeability evaluated with MR imaging. Radiology 2001;218:365–374.
34. White S, Hricak H, Forstner R, et al. Prostate cancer: effect of post-biopsy hemorrhage on interpretation of MR images. Radiology 1995;195:385–390.
35. Ikonen S, Kivisaari L, Vehmas T, et al. Optimal timing of post-biopsy MR imaging of the prostate. Acta Radiol 2001;42:70–73.

Down-Regulation of HLA Class I Antigens in Prostate Cancer Tissues and Up-Regulation by Histone Deacetylase Inhibition

Hiroshi Kitamura,* Toshihiko Torigoe, Hiroko Asanuma, Ichiya Honma, Noriyuki Sato and Taiji Tsukamoto

From the Departments of Urology (HK, IH, TT) and Pathology (HK, TT, HA, IH, NS), Sapporo Medical University School of Medicine, Sapporo, Japan

Purpose: HLA class I down-regulation in cancer cells confers immunological escape from cytotoxic T lymphocytes. We assessed the frequency of down-regulation of HLA class I antigens in a large series of prostate cancer tissues and determined the mechanism of up-regulation by investigating prostate cancer cell lines.

Materials and Methods: Immunohistochemical staining for HLA class I was done in specimens of 419 prostate cancers. We also investigated clinicopathological parameters, and the relationships between HLA class I down-regulation and the parameters. Furthermore, we examined whether HLA down-regulation was caused by epigenetic changes in vitro.

Results: HLA class I was down-regulated in 311 prostate cancers (74.2%) and it significantly correlated with β2-microglobulin down-regulation and a higher clinical stage. Flow cytometric analysis revealed a low level of HLA class I in LNCaP cells, which was up-regulated by the histone deacetylase inhibitor trichostatin A (Sigma®). Trichostatin A up-regulated LNCaP β2-microglobulin at the protein level. Furthermore, chromatin immunoprecipitation assay using an anti-acetylated histone H3 antibody provided direct evidence that trichostatin A up-regulated β2-microglobulin by modulating the acetylation status of the promoter region in LNCaP cells.

Conclusions: The current study shows that the prevalence of HLA class I down-regulation is high in prostate cancer but histone deacetylase inhibitors can up-regulate HLA class I in LNCaP cells by up-regulating β2-microglobulin. We suggest that the combination of an immunotherapeutic approach and histone deacetylase inhibition would accentuate the effects of current immunotherapies for prostate cancer.

Key Words: prostate, prostatic neoplasms, histocompatibility antigens class I, beta 2-microglobulin, trichostatin A

In recent years there have been many studies of specific immunotherapies for various cancers. The rationale for such studies has been supported by strong cellular immune responses, ie introducing cancer specific CTLs from patients. Immune cells must be activated at the tumor site to manifest appropriate effector mechanisms, such as direct lysis or cytokine secretion capable of causing tumor destruction, in addition to the need for a sufficient number of the cells.[1] Most studies showed successful results of in vitro cytotoxicity assays and clinical monitoring, eg by tetramer assay or ELISpot assay (R & D Systems®). However, there have been many cases in which no clinical response was achieved regardless of good immune responses in such assays. Therefore, it is vitally important to evaluate tumor cell factors that influence the clinical responses of specific immunotherapies. Antigen presentation in tumor cells is essential to destroy them, even if an immunotherapy has an excellent effect in eliciting an immune response.

HLA class I has a critical role in the recognition and lysis of tumor cells by CTLs, and defects in antigen presentation could allow the tumor to escape killing by CTLs.[2] The tools for assessing HLA class I expression in surgically removed specimens are limited, although the molecular defects of HLA class I have been studied in detail.[3,4] Recently we developed an excellent mAb for HLA class I, EMR8-5, which is reactive with heavy chains in formalin fixed, paraffin embedded tissue sections. This pan-HLA antibody reacts with all alleles of HLA-A, B and C.

In this study we assessed the frequency of down-regulation of HLA class I antigens using EMR8-5 in a large series of prostate cancer tissues. Furthermore, we determined the mechanism of up-regulation by investigating prostate cancer cell lines.

MATERIALS AND METHODS

Patients and Tissue Samples

We reviewed the clinical pathology archives of 508 consecutive patients who underwent prostate resection or biopsy and were diagnosed with prostatic adenocarcinoma at the Sapporo Medical University Hospital, Sapporo, Japan from 1995 to 2005. Patients whose medical records were incom-

Submitted for publication November 9, 2006.

Study received approval from the university Institutional Review Board for Clinical Research.

Supported by the Stiftelsen Japanese-Swedish Cooperative Foundation and Grant-in-Aid 17390441 from the Japan Society for the Promotion of Science.

* Correspondence and requests for reprints: Department of Urology, Sapporo Medical University School of Medicine, South 1 West 16, Chuo-ku, Sapporo 060-8543, Japan (telephone: 81-11-611-2111, extension 3472; FAX: 81-11-612-2709; e-mail: hkitamu@sapmed.ac.jp).

0022-5347/07/1782-0692/0
THE JOURNAL OF UROLOGY®

Vol. 178, 692-696, August 2007
Printed in U.S.A.
DOI:10.1016/j.juro.2007.03.109

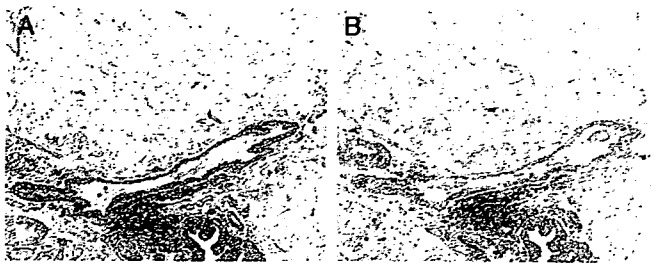

FIG. 1. Representative immunohistochemical staining of HLA class I and β2M down-regulation (score 1) in 68-year-old patient with PSA 5.22 ng/ml and Gleason 4 + 3, clinical T2aN0M0, AJCC stage II prostate cancer shows faint, incomplete membrane staining in cancer cell cytoplasm and/or membranes but complete membrane staining in normal cells, especially lymphocytes and vascular epithelial cells. *A*, staining with mAb for HLA class I (EMR8-5). *B*, staining with mAb for β2M (EMR-B6). Reduced from ×100.

plete were excluded. We selected 419 patients based on the availability of sufficient material for immunohistochemistry. At diagnosis median patient age was 68 years (range 44 to 88) and median serum PSA was 10.9 ng/ml (range 1.1 to 8,670). Informed consent was obtained from patients to use the surgical specimens remaining after pathological diagnosis for the investigational study, which was approved by the Institutional Review Board for Clinical Research at our university. The study included 246 specimens of radical prostatectomy, 136 of prostate biopsy, 28 of cystoprostatectomy for bladder cancer and 9 others, including transurethral prostate resection for benign prostatic hyperplasia, pelvic lymphadenectomy, etc. All hematoxylin and eosin stained slides were reviewed and all of these specimens showed prostatic adenocarcinoma, including Gleason score 3–6, 7–8 and 9–10 in 143, 219 and 57 cases, respectively. Diagnoses were confirmed using the 2002 version of the TNM system. We then classified clinical stage according to the AJCC classification.[5] There were 6 stage I, 320 stage II, 25 stage III and 68 stage IV cases.

Immunohistochemical Staining for HLA Class I

Sections (5 μm) of formalin fixed, paraffin embedded tumors were immunostained after steam heat induced epitope retrieval using mAb EMR8-5, as previously described.[6] We also performed immunohistochemical staining for β2M using our original mAb for β2M, EMR-B6. Human tonsil sections served as positive controls. We also used lymphocytes and vascular epithelium cells in the same specimen as internal positive controls. Negative controls had the primary antibody replaced by buffer. All specimens were reviewed independently using light microscopy by investigators blinded to clinicopathological data (HK and TT).

Membrane immunoreactivity levels for HLA class I and β2M were categorized as undetectable to 2. A score of zero was defined as undetectable staining (fig. 1). A score of 1 was defined as faint, incomplete membrane staining in more than 20% of the tumor cells or as moderate to complete staining in cytoplasm but negative membrane staining in tumor cells. Finally, a score of 2 was defined as complete membrane staining in more than 80% of tumor cells. HLA class I expression was then classified as down-regulated (scores 0 and 1) or positive (score 2).

Statistical Analysis

Spearman's rank correlation was used to test the direction and strength of the relationship between HLA class I expression in cancer cells and other variables, including age, PSA, Gleason score, clinical stage and β2M expression, with $p < 0.05$ considered statistically significant. Calculations were performed using JMP™ software.

Screening of Epigenetic Changes in Prostate Cancer Cell Lines

Treatments with TSA and 5-AC, and flow cytometry. To screen whether HLA class I antigens of prostate cancer cells were down-regulated and whether they could be up-regulated we investigated HLA class I expression on the cell surfaces of prostate cancer cell lines, and the effects of HDAC inhibitor and DNA methyltransferase inhibitor. The human prostate cancer cell lines DU145, PC-3 and LNCaP were cultured in RPMI 1640 supplemented with 10% fetal bovine serum at 37C with 5% CO_2. Cells with fresh medium were treated with TSA at 300 nM for 24 hours as the HDAC inhibitor and with 5-AC (Sigma-Aldrich) at 5 μM for 72 hours as the DNA methyltransferase inhibitor. After cultivation approximately 2×10^6 cells were incubated with mouse anti-HLA class I mAb W6/32 (American Type Culture Collection, Manassas, Virginia) at 4C for 30 minutes, washed twice with PBS and stained with FITC conjugated goat anti-mouse IgG antibody (BD™ Biosciences) at 4C for 30 minutes. The cells were then washed twice with PBS and resuspended in 1 ml PBS. Flow cytometric detection of FITC positive cells was done using a FACSCalibur™ flow cytometer and CELLQuest™ software. An average of 10,000 events was analyzed.

Western Blot Analysis

Western blotting was performed as previously described[7] using the hybridoma supernatants of EMR8-5 and EMR-B6 for HLA class I heavy chain and β2M, respectively, and mAb to β-actin (Sigma).

ChIP Assay

ChIP assay was performed using an Acetyl-Histone H3 Immunoprecipitation Assay Kit (Upstate Biotechnology, Lake Placid, New York) according to the manufacturer protocol. Briefly, cells were plated at a density of 1×10^6 on a 10 cm dish and cultured for 24 hours with 300 nM TSA. Subsequently chromatin was solubilized and subjected to sonication to obtain DNA fragments with an average size of 200 to 1,000 bp. ChIP was performed by incubation with an anti-acetyl histone H3 antibody and a no antibody immunoprecipitation control. Immunoprecipitated DNA served as a template for PCR of β2M promoter. PCR was done in a 50 μl reaction volume using Taq DNA polymerase. Briefly, after heating at 94C for 2 minutes the amplification reaction was performed with primers 5′-GAAAACGGGAAAGTCCC-3′ (forward) and 5′-*AGATCCAGCCCTGGACTAGC*-3′ (reverse) with denaturation at 94C for 30 seconds, annealing at 57C for 30 seconds and extension at 72C for 30 seconds for 30 cycles, followed by incubation at 72C for 7 minutes. For semiquantitative analysis PCR was also performed for

TABLE 1. *Spearman's rank correlation between HLA class 1 expression in cancer cells and other variables*

Variable	Spearman's Rank Correlation Coefficient (ρ)	p Value
Pt age	0.0224	0.6473
PSA	−0.0950	0.0743
Gleason score	−0.0151	0.7575
Clinical stage	−0.1145	0.0191
β2M expression in Ca cells	0.5158	<0.0001

genomic DNA obtained from each sample before immunoprecipitation (fig. 2, Input). The PCR product was visualized with ethidium bromide staining under ultraviolet light after electrophoresis on 2.0% agarose gel.

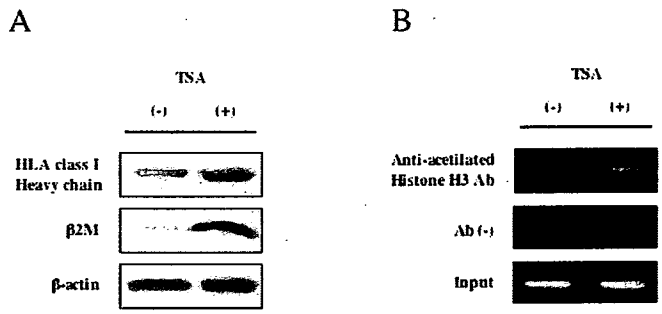

FIG. 2. *A*, Western blotting of LNCaP cells incubated with (+) or without (−) 100 nM TSA for 24 hours. TSA up-regulated β2M protein. *B*, ChIP analysis of histone H3 deacetylation on β2M promoter in LNCaP validated Western blotting result. Input for each reaction served as sample loading internal control. Aliquot precipitated without antibody served as negative control.

RESULTS

Immunohistochemical study of HLA class I in cancer cells revealed that 91, 220 and 108 of the 419 cases had a score of 0, 1 and 2, respectively. In other words, HLA class I was down-regulated in 311 prostate cancers (74.2%). β2M down-regulation was also found in 24.8% of cases, including 59, 256 and 104 with a score of 0 to 2, respectively. Spearman's rank correlation test revealed that HLA class I down-regulation significantly correlated with β2M down-regulation and higher clinical stage (table 1). Table 2 shows clinical stages in the 419 prostate cancers according to HLA class I and β2M expression.

We next investigated whether HLA down-regulation was caused by epigenetic changes in prostate cancer cell lines. Flow cytometric analysis revealed a low level of HLA class I in LNCaP cells, which was up-regulated by TSA but not by 5-AC (Fig. 3). TSA up-regulated LNCaP β2M at the protein level (fig. 2, *A*). Furthermore, ChIP assay using anti-acetylated histone H3 antibody provided direct evidence that TSA up-regulated β2M by modulating the acetylation status of the promoter region in LNCaP cells (fig. 2, *B*).

DISCUSSION

Although HLA class I down-regulation in prostate cancer has been investigated in several studies,[3,8,9] there were some problems, such as an insufficient number of samples, limited distribution of clinicopathological characteristics and method quality. In this study we included a large number of cases and used the mAb EMR8-5, which reacts with more alleles than other antibodies for HLA class I. Furthermore, we classified the immunostaining patterns of HLA class I heavy chain and β2M, considering cell membrane staining, since these factors are important for specific cancer immunotherapy. Our data suggest that immunotherapy such as an HLA class I associated peptide vaccine may not be suitable for more than 70% of patients with prostate cancer. The down-regulation rate was markedly lower than rates in colon, lung, oral cavity, kidney, bladder and liver cancers with 20% to 42% down-regulation (unpublished data). Although various clinical trials of immunotherapies for prostate cancer have recently been done, none of them achieved satisfactory effects regardless of rationally sufficient immunological responses.[10] This study also demonstrated that prostate cancer in patients with a more advanced clinical stage tended to show HLA class I down-regulation more frequently. We suggest that candidates who wish to participate in clinical trials of cancer immunotherapy should undergo immunohistochemical screening for HLA class I expression in the cancer tissue, especially if clinical stage is advanced.

To our knowledge this study revealed for the first time that HLA class I down-regulation strongly correlates with β2M down-regulation in prostate cancer. Furthermore, it showed that LNCaP cells could present characteristics of prostate cancer cell lines, as previously reported,[11] and histone deacetylation might be involved in down-regulation, as demonstrated in in vitro studies using LNCaP cells. Thus, the current results suggest that HDAC inhibitors can up-regulate the HLA class I of prostate cancer. Huang et al reported that β2M activated phosphorylated cyclic adenosine monophosphate element binding protein with increased expression of its target genes, which could enhance tumor growth and angiogenesis, and facilitate the recruitment of osteoblasts and osteoclasts to the site of tumor colonization in bone.[12] In our study 87.8% of the 41 patients with bone metastasis showed β2M down-regulation with a score of 0 to 2 in 10, 26 and 5, respectively. The rate was higher than that in patients without bone metastasis. Our clinicopathological

TABLE 2. *Expression scores of HLA class 1 and β2M in 419 patients with prostate cancer*

		No. HLA Class 1 (%)			No. β2M (%)		
AJCC Stage	Total No.	Score 0	Score 1	Score 2	Score 0	Score 1	Score 2
I	6	0	3 (50.0)	3 (50.0)	0	4 (66.7)	2 (33.3)
II	320	64 (20.0)	169 (52.8)	87 (27.2)	38 (11.9)	196 (61.2)	86 (26.9)
III	25	9 (36.0)	12 (48.0)	4 (16.0)	8 (32.0)	12 (48.0)	5 (20.0)
IV	68	18 (26.5)	36 (52.9)	14 (20.6)	13 (19.1)	44 (64.7)	11 (16.2)
Totals	419	91 (21.7)	220 (52.5)	108 (25.8)	59 (14.1)	256 (61.1)	104 (24.8)

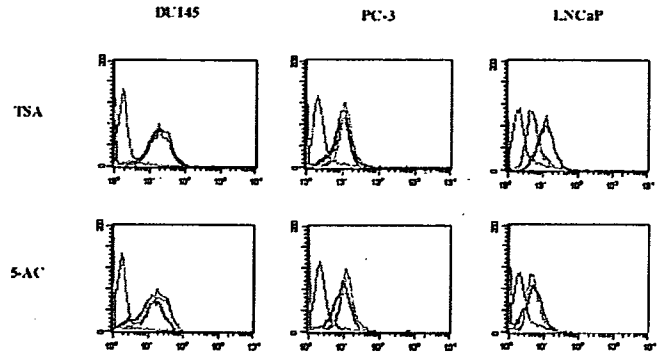

FIG. 3. Prostate cancer cell lines DU145, PC-3 and LNCaP were analyzed for cell surface levels of HLA class I by flow cytometry. Cells were stained with FITC labeled anti-HLA class I antibodies, including neither TSA nor 5-AC (green curves), 100 nM TSA for 24 hours (pink curves) and 5 μM 5-AC for 72 hours (orange curves). Cells were also stained with FITC labeled mouse IgG1 (purple curves). TSA up-regulated HLA class I on LNCaP, whereas 5-AC had no effect on any cell line.

data suggest that β2M expression in prostate cancer cells is not a risk factor for bone metastasis. A reason for the discrepancy between the 2 studies is that Huang et al inoculated human prostate cancer cells into the bone marrow of the host mice, which could be different from the natural history of human prostate cancer. However, we will carefully observe the incidence of bone metastasis, especially in patients in whom cancer tissue shows β2M expression, for a longer time since in vitro study provided evidence that β2M is a growth promoting factor for cancer bone metastasis.[12]

Recently some HDAC inhibitors, eg suberoylanilide hydroxamic acid, were studied in phase I and II trials for hematological and solid tumors.[13–15] Those studies showed that such drugs were well tolerated and could inhibit HDAC activity in tumor tissues with little clinical toxicity.[16] Our data suggest that a combination of an immunotherapeutic approach and HDAC inhibition could accentuate the effects of current immunotherapies for prostate cancer.

CONCLUSIONS

The current study shows that 1) the prevalence of HLA class I down-regulation is high in prostate cancer (especially advanced cancer), 2) HLA class I down-regulation in prostate cancer is related to β2M down-regulation, 3) β2M down-regulation is caused by an epigenetic change in LNCaP cells and 4) TSA can up-regulate HLA class I in LNCaP cells. From these results we suggest that the combination of an immunotherapeutic approach and HDAC inhibition could accentuate the effects of current immunotherapies for prostate cancer.

ACKNOWLEDGMENTS

Emiri Nakazawa and Kumiko Shimozawa provided EMR8-5 and EMR-B6 antibodies. Drs. Yoshihiko Hirohashi and Eiji Sato provided technical assistance.

Abbreviations and Acronyms

5-AC	=	5-azacytidine
β2M	=	β2-microglobulin
AJCC	=	American Joint Committee on Cancer
ChIP	=	chromatin immunoprecipitation
CTL	=	cytotoxic T lymphocyte
FITC	=	fluorescein isothiocyanate
HDAC	=	histone deacetylase
PBS	=	phosphate buffered saline
PCR	=	polymerase chain reaction
PSA	=	prostate specific antigen
TSA	=	trichostatin A

REFERENCES

1. Rosenberg SA, Yang JC and Restifo NP: Cancer immunotherapy: moving beyond current vaccines. Nat Med 2004; **10:** 909.
2. Khong HT and Restifo NP: Natural selection of tumor variants in the generation of "tumor escape" phenotypes. Nat Immunol 2002; **3:** 999.
3. Marincola FM, Jaffee EM, Hicklin DJ and Ferrone S: Escape of human solid tumors from T-cell recognition: molecular mechanisms and functional significance. Adv Immunol 2000; **74:** 181.
4. Seliger B, Cabrera T, Garrido F and Ferrone S: HLA class I antigen abnormalities and immune escape by malignant cells. Semin Cancer Biol 2002; **12:** 3.
5. Prostate. In: AJCC Cancer Staging Manual, 6th ed. Edited by FL Greene, DL Page, ID Flemming, A Fritz, CM Balch, DG Haller et al. New York: Springer 2002; pp 309–316.
6. Kitamura H, Torigoe T, Honma I, Asanuma H, Nakazawa E, Shimozawa K et al: Expression and antigenicity of survivin, an inhibitor of apoptosis family member, in bladder cancer: implications for specific immunotherapy. Urology 2006; **67:** 955.
7. Tsukahara T, Nabeta Y, Kawaguchi S, Ikeda H, Sato Y, Shimozawa K et al: Identification of human autologous cytotoxic T-lymphocyte-defined osteosarcoma gene that encodes a transcriptional regulator, papillomavirus binding factor. Cancer Res 2004; **64:** 5442.
8. Blades RA, Keating PJ, MaWilliam LJ, George NJ and Stern PL: Loss of HLA class I expression in prostate cancer: implications for immunotherapy. Urology 1995; **46:** 681.
9. Zhang H, Melamed J, Wei P, Cox K, Frankel W, Bahnson RR et al: Concordant down-regulation of proto-oncogene PML and major histocompatibility antigen HLA class I expression in high-grade prostate cancer. Cancer Immunol 2003; **3:** 2.
10. Webster WS, Small EJ, Rini BI and Kwon ED: Prostate cancer immunology: biology, therapeutics, and challenges. J Clin Oncol 2005; **32:** 8262.
11. Sanda MG, Restifo NP, Walsh JC, Kawakami Y, Nelson WG, Pardoll DM et al: Molecular characterization of defective antigen processing in human prostate cancer. J Natl Cancer Inst 1995; **87:** 280.
12. Huang WC, Wu D, Xie Z, Zhau HE, Nomura T, Zayzafoon M et al: β2-microglobulin is a signaling and growth-promoting factor for human prostate cancer bone metastasis. Cancer Res 2006; **66:** 9108.
13. Kelly WK, O'Connor OA, Krug LM, Chiao JH, Heaney M, Curley T et al: Phase I study of an oral histone deacetylase inhibitor, suberoylanilide hydroxamic acid, in patients with advanced cancer. J Clin Oncol 2005; **23:** 3923.

14. O'Connor OA, Heaney ML, Schwartz L, Richardson S, Willim R, MacGregor-Cortelli B et al: Clinical experience with intravenous and oral formulations of the novel histone deacetylase inhibitor suberoylanilide hydroxamic acid in patients with advanced hematologic malignancies. J Clin Oncol 2006; **24:** 166.
15. Richon VM: Cancer biology: mechanism of antitumour action of vorinostat (suberoylanilide hydroxamic acid), a novel histone deacetylase inhibitor. Br J Cancer 2006; **95:** S2.
16. O'Connor OA: Clinical experience with the novel histone deacetylase inhibitor vorinostat (suberoylanilide hydroxamic acid) in patients with relapsed lymphoma. Br J Cancer 2006; **95:** S7.

The Prostate 67:1163 – 1173 (2007)

Exploration of Target Molecules for Prostate Cancer GeneTherapy

Kazuhiro Suzuki,[1,2] Kiminori Nakamura,[1] Kazunori Kato,[1] Hirofumi Hamada,[1] and Taiji Tsukamoto[2]*

[1]Department of Molecular Medicine, Sapporo Medical University School of Medicine, Sapporo, Japan
[2]Department of Urology, Sapporo Medical University School of Medicine, Sapporo, Japan

BACKGROUND. Focusing on Adv-FZ33, a modified adenovirus in which a synthetic 33-amino-acid immunoglobulin G-binding domain was inserted into the adenoviral fiber protein, we tried to identify suitable target molecules for prostate cancer-specific gene therapy.
METHODS. Hybridomas were established from mice immunized with prostate cancer cell lines. The hybridomas were screened using Adv-FZ33 to create monoclonal antibodies (mAbs) that induced high gene transfer efficiency for PC-3 cells. Furthermore, we identified target antigens of the mAbs by immunoprecipitation and mass spectrometry, and investigated the expression of target molecules by flow cytometry and immunocytochemistry.
RESULTS. Using Adv-FZ33, we established four different mouse mAbs that increased transduction efficiency for PC-3. The target antigens identified were Ep-CAM, CD155, HAI-1, and Na,K-ATPase β1. These antigens were expressed in several cancer cell lines, including prostate cancer. Human prostatic myofibroblast cells lacked expression of Ep-CAM and HAI-1.
CONCLUSIONS. We established anti-Ep-CAM mAb and anti- HAI-1 mAbs. Gene transduction via Ep-CAM and HAI-1 may be a novel strategy for treatment of prostate cancer. *Prostate 67: 1163–1173, 2007.* © 2007 Wiley-Liss, Inc.

KEY WORDS: **gene therapy; modified adenovirus vector; prostate cancer; monoclonal antibody**

INTRODUCTION

Prostate cancer is the most common cancer in the West and the second leading cause of male cancer-related death [1]. Advanced androgen-insensitive prostate cancer exhibits little or no response to conventional therapies [2]. Thus, gene therapy is anticipated as an alternative treatment for this type of disease [3].

Adenoviral vectors are commonly used in gene therapy. This is due to their ability to produce high titers and infect various cell types [4]. Genes are transferred to target cells via the Coxsackie adenovirus receptor (CAR), which is a cell-surface receptor required for adenovirus attachment [5]. However, because CAR is widely expressed on normal cells, its lack of specificity is still an obstacle for its clinical application in cancer-gene therapy. In this context, we focused on the function of fiber Z33 type adenovirus (Adv-FZ33). This adenovirus has a synthetic 33-amino-acid immunoglobulin G (IgG)-binding domain (Z33) derived from staphylococcal protein A inserted into the virus having fiber protein [6]. This modified fiber binds IgG with high affinity and allows an antibody to redirect the vector to a new target molecule on the cell surface.

In this study, we established hybridomas from mice splenocytes immunized with prostate cancer cell lines. Then we selected from them monoclonal antibodies

Grant sponsor: Stiftelsen Japanese-Swedish Research Foundation; Grant sponsor: Cancer Research from the Ministry of Health and Welfare of Japan; Grant sponsor: Ministry of Education, Culture, Sports, Science and Technology.

*Correspondence to: Taiji Tsukamoto, MD, Department of Urology, Sapporo Medical University School of Medicine, S-1, W-16, Chuo-Ku, Sapporo 060-8543, Japan. E-mail: taijit@sapmed.ac.jp

Received 12 January 2007; Accepted 4 April 2007
DOI 10.1002/pros.20613
Published online 21 May 2007 in Wiley InterScience (www.interscience.wiley.com).

(mAbs) that increased transduction efficiency by bridging Adv-FZ33 with prostate cancer.

MATERIALS AND METHODS

Cell Lines

We used human prostate cancer cell lines (PC-3, LNCaP, and DU145), a human renal cell carcinoma cell line (Caki-1), a bladder cancer cell line (T24), an ovarian cancer cell line (SKOV-3), normal dermal fibroblasts (PDF), normal prostate myofibroblasts (PrMFB), human embryonic kidney cells (293 T), and mouse myeloma (P3U1). These cell lines were purchased from American Type Culture collection (Manassas, VA). PrMFB was established in our department [7]. Cells were cultured in RPMI-1640 supplemented with 10% fetal calf serum, 1% non-essential amino acids, 1 mm sodium pyruvate, and 1% streptomycin/penicillin solution.

Adenoviral Vectors

We generated adenoviral vectors containing the IgG-binding Z33 motif from Staphylococcal protein A at the HI-loop of the adenovirus type 5 (Ad5) fiber knob, and designated it Adv-FZ33 (represented in Fig. 1A). Details of Adv-FZ33 construction were described in a previous study [8].

Production and Screening of Hybridomas

Screening protocol for targeting mAbs is represented in Figure 1C. A Balb/c mouse was injected intraperitoneally with a mixture of PC-3, LNCaP, and DU145 cells (total: 2×10^6) every 14 days. Three days after the 5th injection, the mouse was sacrificed and 1×10^8 mouse splenocytes were fused with 2×10^7 P3U1 cells using polyethylene glycol (PEG). When hybridomas grew to about 50% confluence, culture supernatants were tested for antibody activity. PC-3

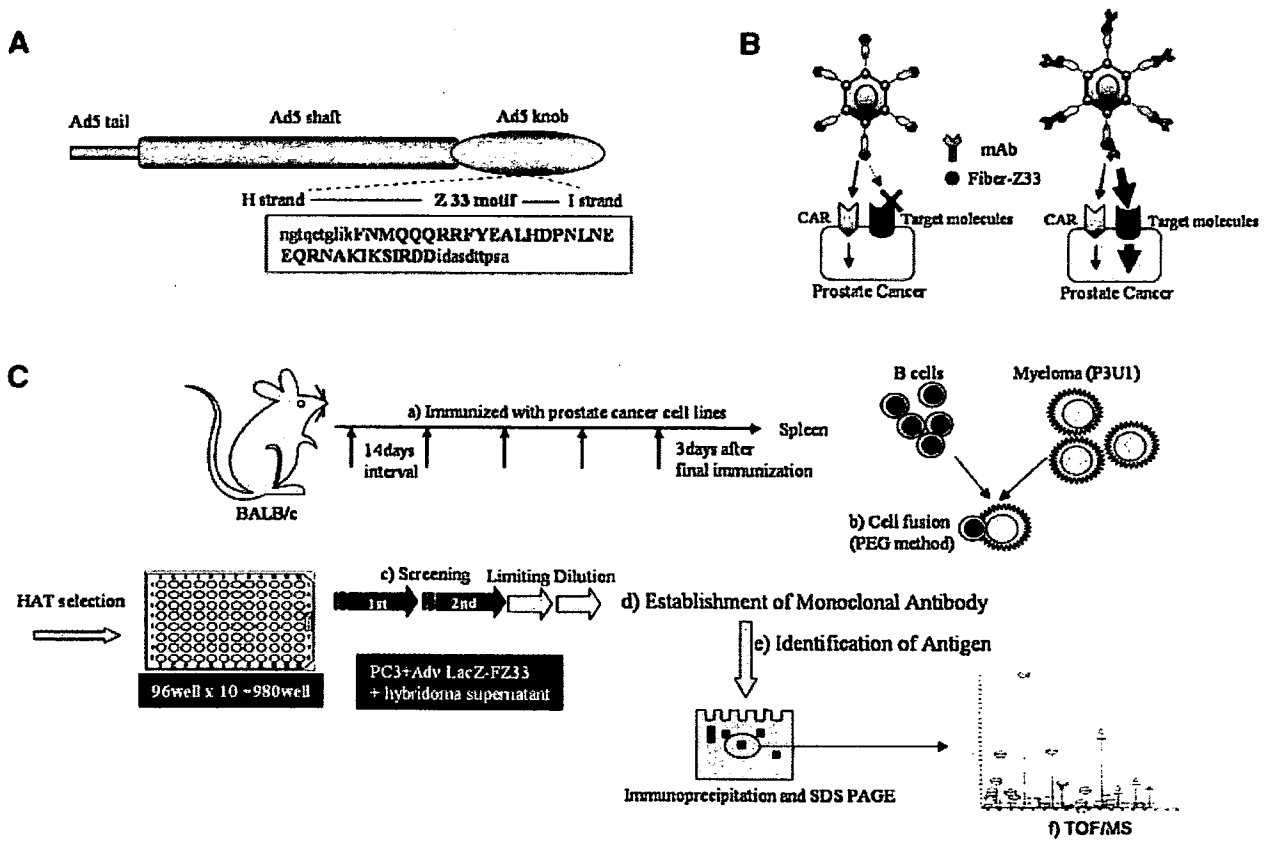

Fig. 1. Schematic representation of Adv-FZ33 and procedure for the establishment of cancer-targeting antibodies. **A**: Z33-modified Ad5 fiber A synthetic 33-amino acid IgG-binding domain (Z33), derived from staphylococcal protein A, was inserted into the HI loop of knob protein. **B**: Targeting with Adv-FZ33 Adv-FZ33 binds immunoglobulins and allows an antibody to redirect the vector to a new target molecule on the cell surface. Our Adv-FZ33 had intact CAR-binding structure and retained CAR-binding ability. **C**: Methods for establishment of novel cancer-targeting antibodies using Adv LacZ-FZ33. (a) Immunization with prostate cancer cell lines. (b) Cell fusion with PEG method. (c) Screening and limiting dilution. (d) Establishment of monoclonal antibody. (e) Identification of antigen by immunoprecipitation and SDS–PAGE. (f) Detection of molecule by mass spectorometry.

cells were prepared in 96-well microplates. After the removal of the culture medium, supernatants were added to each well and incubated for 1 hr at 4°C, after which supernatants were removed and microplates were washed with PBS. Adv-FZ33 inserted LacZ reporter gene (Adv LacZ -FZ33) prepared in FBS-free RPMI-1640 at a multiplicity of infection (MOI) of 1,000 vp/cell was added to each well and incubated for 1 hr at 4°C. Then microplates were washed twice with PBS and incubated at 37°C in a 5% CO_2 incubator. Twenty-four hours after infection, chemiluminescent β-Gal reporter gene assays (Roche Diagnostics, Mannheim, Germany) were performed according to the company's recommendations. Hybridomas that showed high β-Gal activity were picked through first and second screenings and cloned by twice limiting dilution. These hybridomas were injected into nude mice intraperitoneally. The mouse monoclonal antibody was purified from ascites of nude mice using protein G sepharose beads (Amersham Bioscience, Uppsala, Sweden). A commercial kit (Roche Diagnostics) was used to detect the isotypes of antibodies.

Identification of Target Molecules

Immunoprecipitation of biotinylated protein and detection of molecular weight. First, 2×10^6 PC-3 cells were prepared and the cell surface was biotinylated (PIERCE, Rockford, IL). Membranes were solubilized on ice for 30 min in 1 ml of buffer containing 1% NP40, 50 mM Tris-HCl, pH 7.6, 150 mM NaCl, and protease inhibitor cocktail (Roche Diagnostics). Samples were cleared of nuclear fragments by centrifugation for 20 min at 15,000*g* at 4°C, then mixed with protein G sepharose beads and incubated for 2 hr at 4°C, after which the beads were centrifuged to remove non-specifically bound proteins. Five μg of the mAbs established in this study and control mouse IgG (eBioscience, San Diego, CA) were added to the supernatant of each sample and allowed to incubate for 2 hr at 4°C. The immunocomplexes were precipitated by addition of protein G sepharose beads to each sample and incubated for 2 hr at 4°C. The supernatant was discarded and the beads were washed six times with solubilization buffer. Immunocomplexes binding with beads were boiled for 5 min in 20μl of SDS sample buffer containing 5% 2-mercaptethanol. Samples were separated using 5–20% gradient polyacrylamide gels (BioRad, Hercules, CA) and transferred onto nitrocellulose membranes (Millipore, MA). After blocking with 5% milk in TBS consisting of 10 mM Tris-HCl (pH 7.5), 150 mM sodium chloride, and 0.05% Tween-20, the membranes were incubated for 1 hr at room temperature with avidin-horseradish peroxidase (dilution 1:2,000; Amersham Bioscience, Buckinghamshire, England). Detection was carried out by enhanced chemiluminescence (Amersham Bioscience) according to the manufacturer's instructions.

Silver stain and mass spectrometry. For this procedure, 1×10^9 PC-3 cells were solubilized in 40 ml of buffer as described above. After the removal of nuclear fragments by centrifugation, samples were mixed with protein G sepharose beads and incubated overnight at 4°C to remove non-specifically bound proteins. Five micrograms of the mAbs established in this study and control mIgG1 were added to the supernatant of each sample and allowed to incubate for 2 hr at 4°C. The immunocomplex was precipitated by addition of protein G sepharose beads to each sample and incubated for 2 hr at 4°C. Samples were separated by SDS–PAGE as described above. The polyacrylamide gel was stained using a Silver Stain kit (Wako Pure Chemical Industries, Ltd, Osaka, Japan) according to the company's recommendations. Specifically stained protein bands were extracted from the gel, digested by trypsin, and analyzed by oMALDI-Qq-TOF MS/MS QSTAR Pulsari (Applied Biosystems Japan Ltd, Tokyo, Japan).

Confirmation of results of mass spectrometry. The cDNAs of target molecules identified by mass spectrometry were synthesized by reverse transcription or obtained from Open Biosystems, Inc. (Huntsville, AL). Some cDNAs were ligated into the expression vector with pTarget vector (Promega, Madison, WI) or pcDNA3.1(+) vector (Invitrogen, Carlsbad, CA). cDNA was transfected into 293 T cells or CHO cells using Lipofect AMINE Plus reagent (Invitrogen). Forty-eight hours after transfection, transfected cells were washed and then suspended in staining medium (2% FBS/PBS) containing saturating amounts of mAbs established in this study and negative control IgG1 (MOPC-21, BD PharMingen, San Diego, CA) as controls. The reactivity of each mAb was analyzed by flow cytometry using a FACS-Calibur™ (Becton Dickinson, San Jose, CA).

Transduction Efficiency in PC-3

Flow cytometric analysis. To examine transduction efficiency using Adv-FZ33 with established mAbs, PC-3 cells were prepared in six-well plates at the concentration of 1×10^5 cells/well. After removal of the culture medium, FBS-free RPMI-1640 containing the mAbs created in this study at a concentration of 2 μg/ml was added to each well and incubated for 1 hr at 4°C. Adv-FZ33 inserted the DNA fragment encoding

the enhanced green fluorescence protein (Adv EGFP - FZ33) prepared in FBS-free RPMI-1640 at the MOI of 1,000 vp/cell was added to each well and incubated for 1 hr at 4°C. Then the wells were washed twice with PBS and incubated at 37°C in a 5% CO_2 incubator. Twenty-four hours after infection, cells were collected and their transduction efficiencies were analyzed by flow cytometry using a FACS-Calibur®.

Chemiluminescent β-Gal reporter gene assay. PC-3 cells were prepared in 96-well plates at the concentration of 5×10^3 cells/well and divided into five groups by the concentration of the mAbs and control IgG1, that is 0.001, 0.01, 0.1, 1.0, and 10 μg/ml. After removal of the culture medium, 50 μl of FBS-free RPMI-1640 at the concentrations of the mAb described above was added to each well and incubated 1 hr at 4°C. Medium was removed and microplates were washed with PBS. Fifty microliters of Adv LacZ-FZ33 at MOI of 1,000 vp/cell prepared in FBS-free RPMI-1640 was added to each well and incubated for 1 hr at 4°C. The microplates were then washed twice with PBS and incubated at 37°C in a 5% CO_2 incubator. Twenty-four hours after infection, chemiluminescent β-Gal reporter gene assays were performed. Furthermore, we compared transduction efficiency of Adv-FZ33 with wild type adenovirus (Ad5). The concentration of virus was divided into 30, 100, 300, 1,000, 3,000, and 10,000 vp/cell. The concentration of mAb and control IgG1 was 1 μg/ml.

Distribution of Target Antigens

Flow cytometric analysis. The reactivity of the mAbs with human cell lines (PC-3, LNCaP, DU145, Caki-1, T24, SKOV-3, PDF, and PrMFB) was analyzed by flow cytometry. Cells in the logarithmic growth phase were tripsinized and washed. A cell pellet containing 1×10^5 cells was suspended in staining medium (2% FBS/PBS) containing 2 μg of mAb or isotype control IgG as controls for 60 min at 4°C in the dark. After three rinses with PBS, cells were incubated with a fluorescein isothiocyanate (FITC)-conjugated rabbit anti-mouse Ig antibody (diluted 1:100) (TAGO, Inc., Burlingame, CA) for 45 min at 4°C. The cell suspension obtained was washed three times with PBS and then analyzed by flow cytometry.

Immunohistochemistry. Study specimens of 30 patients were selected from the clinical pathology archives of the Sapporo Medical University Hospital. They included 30 specimens consisting of 13 needle-core biopsies, 14 prostatectomies, and 3 cystoprostatectomies obtained between 2001 and 2002. All H&E-stained slides were reviewed and the respective diagnoses were confirmed. All of these specimens included prostatic adenocarcinoma (22 patients with Gleason scores of 5–8, and 8 with Gleason scores of 9).

Immunohistochemistry with mAbs created in this study was performed on 5-μm thick, formalin-fixed paraffin-embedded tissue sections mounted on poly L-lysine-coated slides. The concentration of the mAb as the primary antibody was 5 μg/ml. Details of immunohistochemistry methods were described in a previous study [9].

RESULTS

Establishment of Hybridomas and Mouse Monoclonal Antibodies

Cell fusions done three times produced hybridoma colonies in 2,500 wells. We cloned the hybridomas from wells with high β-Gal activity by limiting dilution, because the β-Gal activity of each well reflected the transfection efficiency into PC-3 cells via the antigen recognized by the antibodies secreted from the hybridoma. We thereby established hybridomas secreting mAb 1B7, 2H7, 6F8, and 9B10. Isotypes of mAb 1B7, 2H7, and 6F8 were determined to be IgG1 kappa and, for mAb 9B10, IgG2a kappa.

Identification of mAbs 1B7, 2H7, 6F8, and 9B10 Antigens

Biotinylated proteins were detected at 40 kDa by immunoprecipitation using mAb 1B7 (Fig. 2A). Silver stain detected the same proteins. The epithelial cell adhesion molecule (Ep-CAM) was detected by mass spectrometry (Fig. 2B,C). cDNA of Ep-CAM was transfected into 293 T cells. Flow cytometry revealed that mAb 1B7 reacted with transfectants expressing Ep-CAM (Fig. 2D). We therefore concluded that the antigen recognized by mAb 1B7 was Ep-CAM.

In immunoprecipitation using mAb 2H7, an 80 kDa protein was detected (Fig. 3A). The protein was identified as poliovirus receptor (CD155) by mass spectrometry (Fig. 3B,C). cDNA of human CD155 was transfected into CHO cells and mAb 2H7 reacted with cells expressing CD155 (Fig. 3D).

In immunoprecipitation using mAb 6F8, 110, and 50 kDa biotinylated proteins were detected (Fig. 4A). The 110 kDa silver-stained protein, which was sharper than the 50 kDa band, was extracted and analyzed by mass spectrometry (Fig. 4B,C). The protein was identified as Na,K-ATPase β1. We obtained the cDNAs of human Na,K-ATPase α1, Na,K-ATPase α2, Na, K-ATPase α3, Na,K-ATPase α4 transcript variant 2, Na, K-ATPase β1, Na,K-ATPase β2, and Na,K-ATPase β3 to determine the antigens. Each cDNA was transfected into CHO cells and it was found that mAb6F8 reacted

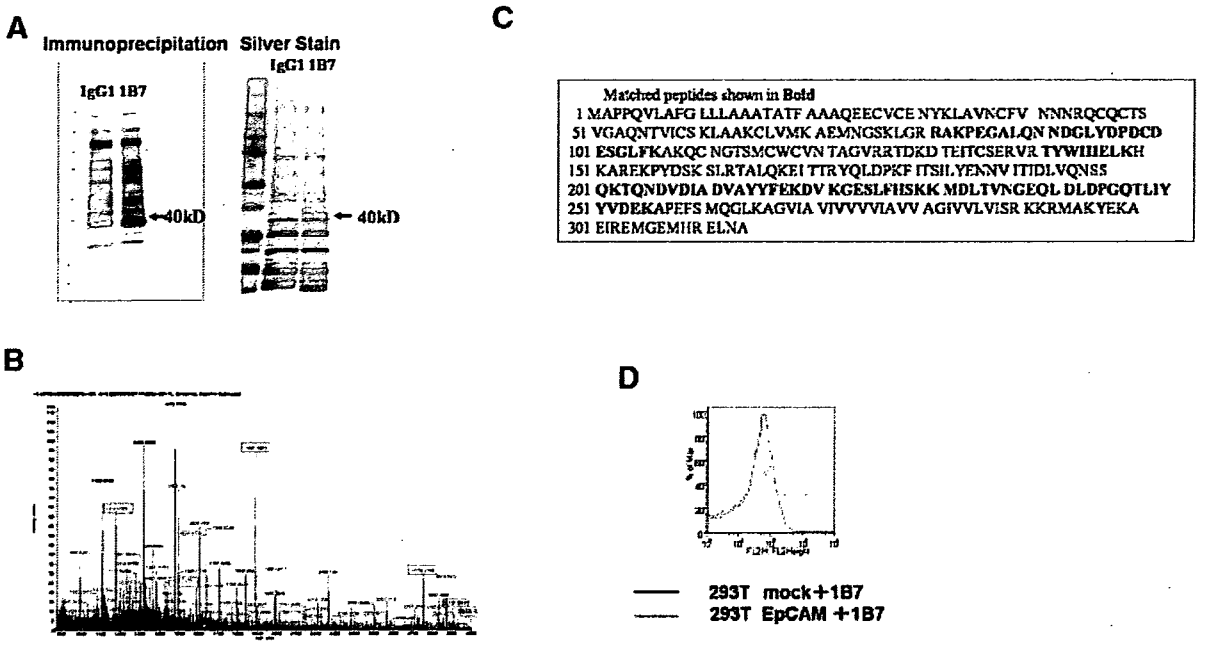

Fig. 2. Identification of mAb 1B7 antigen. **A**: Lysates of PC-3 cells were immunoprecipitated with mAb 1B7; proteins (40 kDa) were detected. The band that appeared at 40 kDa (indicated by an arrow) was excised from the gel and analyzed by mass spectrometry. **B**: High-intensity spectra indicated by a rectangles indicate the peptide, the sequence of which corresponded to the amino acid sequence of human Ep-CAM. **C**: Boldface indicates the sequence of the detected peptide. **D**: Flow cytometry of the reactivity of mAb 1B7 with 293T cells transfected with cDNA of Ep-CAM. mAb 1B7 reacted only with 293T cells transfected with cDNA of Ep-CAM.

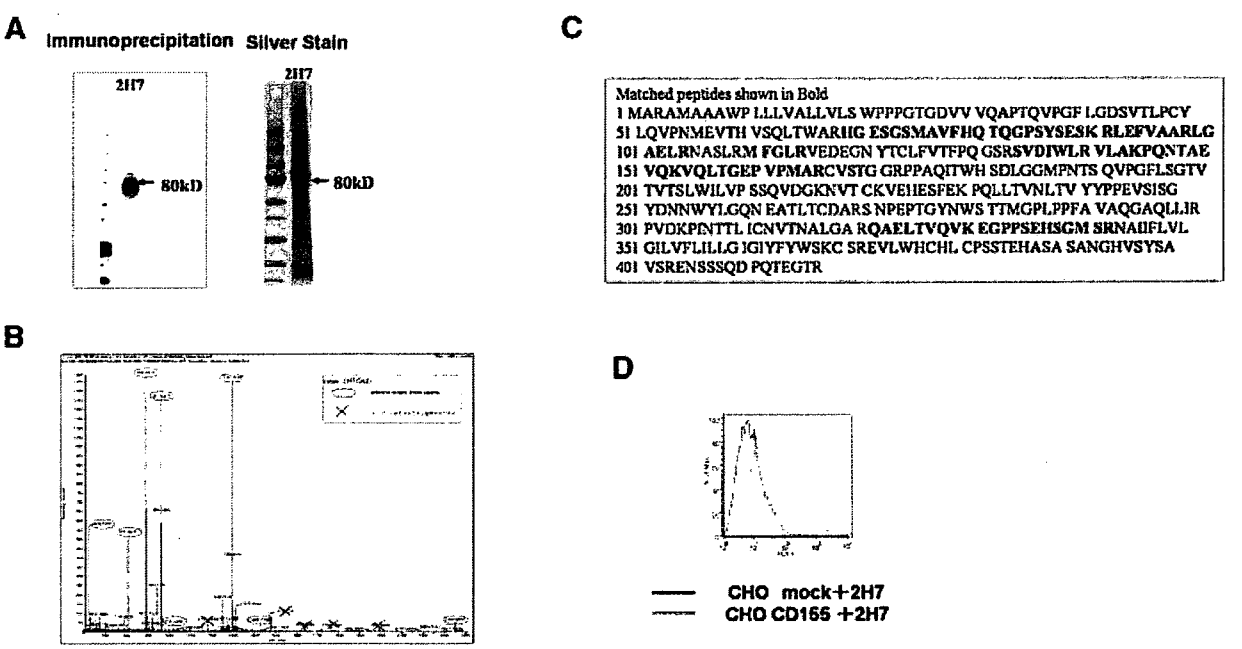

Fig. 3. Identification of mAb 2H7 antigen. **A**: Immunoprecipitation with mAb 2H7. The band that appeared at 80 kDa (indicated by an arrow) was excised from the gel and analyzed by mass spectrometry. **B**: Encircled high-intensity spectra indicate the peptide, the sequence of which corresponded to the amino acid sequence of human CD155. **C**: Boldface indicates the sequence of the detected peptide. **D**: Flow cytometry of the reactivity of mAb 2H7 with CHO cells transfected with cDNA of CD155. mAb 2H7 reacted only with CHO cells transfected with cDNA of CD155.

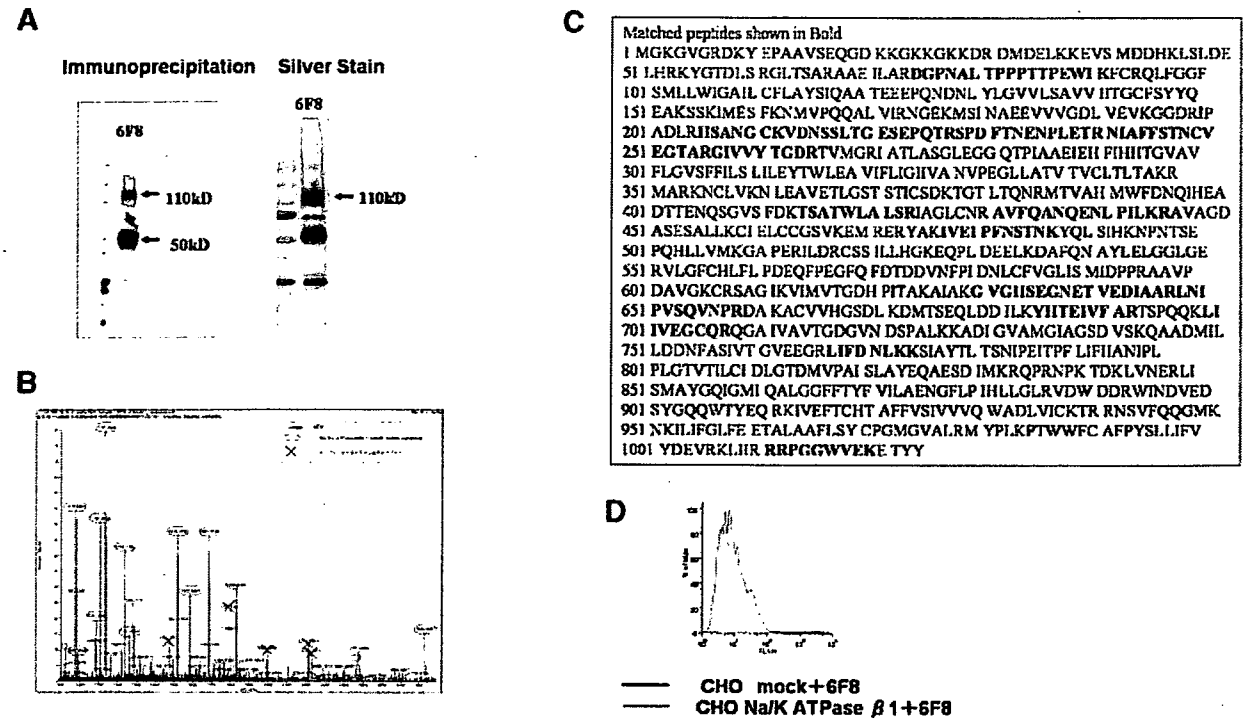

Fig. 4. Identification of mAb 6F8 antigen. **A**: immunoprecipitation with mAb 6F8; proteins (110 and 50 kDa) were detected. The band that appeared at 110 kDa was excised from the gel and analyzed by mass spectrometry. **B**: Encircled high-intensity spectra indicate the peptide, the sequence of which corresponded to the amino acid sequence of human Na,K-ATPase αI. **C**: Boldface indicates the sequence of the detected peptide. **D**: Flow cytometry of the reactivity of mAb 6F8 with CHO cells transfected with the cDNA of each subunit and isozyme of human Na,K-ATPase. mAb 6F8 reacted only with CHO cells transfected with cDNA of human Na,K-ATPase βI.

only with the transfectant expressing the Na,K-ATPase β1 subunit (Fig. 4D). We therefore concluded that the antigen recognized by mAb 6E3 was Na,K-ATPase β1.

In immunoprecipitation using mAb 9B10, a 55 kDa protein was detected (Fig. 5A). The protein was identified as HAI-1 by mass spectrometry (Fig. 5B,C). cDNA of human hepatocyte growth factor activator inhibitor type 1 (HAI-1) transcript variant 2 and HAI-1 transcript variant 3 were obtained. Each cDNA was transfected into CHO cells. mAb 9B10 reacted with each transfectant (Fig. 5D). Therefore, we concluded that mAb 9B10 recognized HAI-1.

Transfection Efficiency Into PC-3 With mAbs and Adv-FZ33

Flow cytometric analysis. Transfection efficiency was evaluated with various mAbs. Cells transfected using AdvEGFP-FZ33 together with mAb 1B7, 2H7, 6F8, and 9B10 showed enhanced expression EGFP compared with those together with mouse IgG1 (Fig. 6A).

Chemiluminescent β-Gal reporter gene assay. β-Gal activity in mAb 1B7, 2H7, and 6F8 at the concentration 1.0 μg/ml showed about 70-fold enhancement compared with control mouse IgG1. In mAb 9B10, transfection efficiency showed about 10-fold enhancement (Fig. 6B). Adv LacZ-FZ33 with mAb 6F8 showed significantly high expression of β-Gal compared with wild type—fiber adenovirus with or without mAb (Fig. 6C).

Distribution of Target Antigens

Expression in several cell lines. We examined the reactivities of mAb 1B7, 2H7, 6F8, and 9B10 with cancer and non-cancer cell lines by flow cytometry. mAb 2H7 and 6F8 reacted strongly with all cell lines (Fig. 7B,C). mAb 1B7 reacted with all cancer cell lines but not with PrMFB and PDF (Fig. 7A). mAb 9B10 did not react with SKOV-3, PrMFB, or PDF (Fig. 7D).

Histologic findings on the specimens. All of the prostate cancer cells (Fig. 8A,C) and most of the normal epithelial cells (Fig. 8B) showed strong immunoreactivity for mAb 1B7 in all the samples. Some of the normal epithelial cells (Fig. 8C,D) and all of the stromal cells (Fig. 8A–D) showed negative staining. No samples were stained with the other three mAbs.